Final report

1.1 Project details

Project title	Harmonized Integration of Gas, District Heating and Electric Systems
Project identification (program abbrev. and file)	HIGHE (No. 12220)
Name of the programme which has funded the project	ForskEL
Project managing company/institution (name and address)	Aalborg University, Aalborg, Denmark
Project partners	AAU-ET, AAU-PLAN, NTNU, Ramboll
CVR (central business register)	DK20342536
Date for submission	2017.12.17

1.2 Short description of project objective and results

The integration natural gas, district heating, and electrical systems are attracting increasing attention with the increasing use of renewable energy. However, the energy distribution systems are conventionally planned and operated independently. There is no such experience on how to plan and how to optimally operate the distribution systems integrated with multiple energy carriers, which may result in the reduced returns of the investment. This project timely addresses two main problems: system planning and operation. The project has developed strategies, models and methods for systemically planning and coordinative optimal operation of the energy systems with multi-carriers in order to realise a flexible, clean, efficient and secured overall energy system.

Integrationen af naturgas, fjernvarme og el-systemer tiltrækker øget opmærksomhed med det stigende forbrug af vedvarende energi. Energi distribueringssystemerne er dog traditionelt planlagt og drives uafhængigt. Der er ingen erfaring med at planlægge og optimere driften af distributionssystemerne integreret med flere energibærere, hvilket kan resultere i et reduceret afkast af investeringen. Dette projekt omhandler helt aktuelt to store problemer: systemplanlægning og drift. Projektet har udviklet strategier, modeller og metoder til systemisk planlægning og koordinerende optimal drift af energisystemerne med multibærere for at realisere et fleksibelt, rent, effektivt og sikret overordnet energisystem.

1.3 Executive summary

The capacity of the coal-fired central power plants are reducing and that of the intermittent renewable resources like wind power are increasing. Large-scale application of renewable energy based generation units brings clean environment benefit but the associated fluctuating power presents challenges to the balance between power generation and consumption, which threatens the power grid security. Renewable power generation, such as wind power, may not be flexibly controlled and has a very different profile from the normal electricity load curve, while power grid itself does not have very much energy storage capacity. Existing electrical

energy storage technologies may not yet be able to cost effectively balance the power shortfalls and surpluses of generation fluctuations of wind energy and other renewable energies. Consequently, the curtailments of the renewable power may happen in the situations of large-scale renewable integration, which results in the waste of renewable energy. One possible solution is to interconnect together the energy systems with quite different characteristics, such as electricity, gas and thermal systems to balance the overall energy generation and consumption in the interconnected system, so that the fluctuating renewable energy may be more effectively exploited. However, the concepts of the integrated energy system with renewables is relatively new, many unknowns need to be treated, system planning and optimal operation are two main issues.

The project of Harmonized Integration of Gas, Heat and Electric systems (HIGHE) has been conducted to provide comprehensive solutions to the system planning and operation strategies of the energy systems with multiple energy carriers. This project aims at developing strategies, models and methods to realize the optimised planning and operation of integrated energy systems, including electricity, gas and heating, so as to accommodate the fluctuated renewables and to establish an efficient and clean energy system.

The project consists of two work packages to deal with the planning issue and operation topic respectively. The project main aspects include: models of energy sources and energy carrier networks, optimal energy flow, and strategies and methods of network expansion planning and optimal operation. The project has been conducted as planned, more specifically, following direct technical results have been obtained.

- The stochastic models of energy profiles have been built for techno-economic evaluation.
- The network models for future expended energy system have been built.
- Based on the network models, risk assessment and mitigation methods have been proposed.
- The multi-objective optimization for network design and expansion has been performed.
- The optimal energy flow model for integrated energy systems has been developed.
- The multi-time period optimization has been carried out.
- The coordination of various devices has been optimized to improve the reliability, efficiency and sustainability of the overall system.
- A software tool for coordination of the integrated energy systems has been developed and is being implemented on line.

Finally, the online tool has been developed for the.

With the above results, the two main objectives in this project: optimal planning and operation methods have been achieved. The major achievements are highlighted in an order of development steps in Fig. 1. Their technical details are described in the Section 1.5.1.

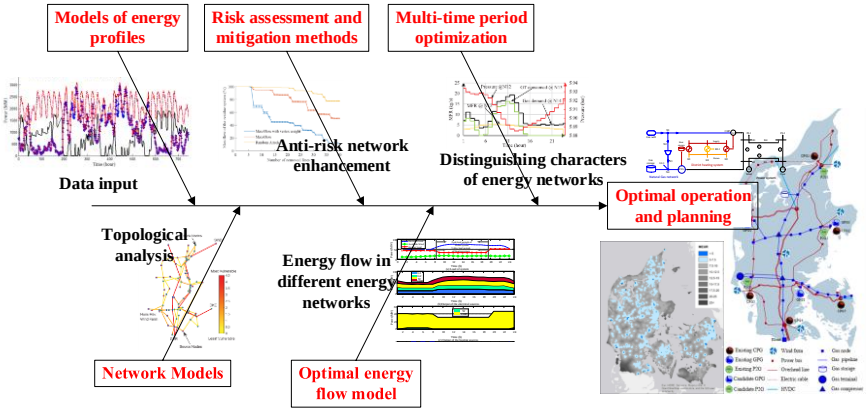

Fig. 1 Overview of the project evolution.

It is expected that the project results can provide very useful concepts, models, methods and tools, to the energy system developers and operators, including operators of power grid, gas system and heating system, and equipment manufacturers and plant owners for considering the system planning in long-term as well as make daily operation schedule in energy markets. The utilization of the project results can lead to the improved efficiency of energy distribution, improved returns on the investment for the infrastructure, and can increase the utilization of intermittent renewable energy and further reduce the fossil fuel dependency and greenhouse gas emission, and present more opportunity for renewables, like increasing wind power integration and utilization. Eventually, it contributes to the development of an environmental friendly, efficient and sustainable energy system.

1.4 Project objectives

1.4.1 The project objectives and implementations

The project is organised into two work packages, with the following objectives recalled from the project proposal:

- Evaluate the techno-economic aspects of energy system with multiple energy carriers
- Develop the network expansion model and topological analysis of integrated gas, heating/cooling and electric systems.
- Conduct the risk assessment for the network.
- Propose the system expansion planning model and optimization approach
- Develop models and algorithm for determining the optimal energy flows of the integrated energy systems
- Develop optimization method for coordinated operation of the integrated energy system with consideration of temporal spatial correlations
- Propose emergency control strategies to improve the reliability and secure energy supplies.
- Develop an online software tool for coordinated operation of the integrated energy systems.

WP1 addresses the first four objectives, and WP2 treats the rest four objectives. The major implementation of the project is presented as follows in according to the work tasks.

Work Package 1 -- System design and network expansion planning for the gas/electric coordinated systems.

WP1.1 Stochastic energy profiles models for techno-economic evaluation

In this working task, the method to model the characteristics of energy consumption and renewable energy production, combining the self-organizing maps and hidden Markov model

(HMM), has been developed as detailed in Section 1.5.1.1. The model is used to evaluate the techno-economic feasibility of utilization of renewable energies based electricity to produce gas in practical energy distribution systems. One conference paper has been published based on the work.

WP1.2 Network models and topological analysis for future expended energy system analysis and evaluation

In WP1.2, the topological analysis is performed with advanced complex network based approach. The critical scenarios are identified by using the principal component analysis (PCA) and convex hull. The proposed method is validated on western Danish power system.

WP1.2 has closely linked with below WP1.3 where the developed models and topological analysis methods have been used to assess the risk caused by intentional attacks on the power grid. Simulation results demonstrate the effectiveness of the method and have been compared with the planning strategy from the transmission system operator. The details are introduced in Section 1.5.1.2. One journal paper has been published according to the results.

WP1.3 Analyze of the low-probability but high-impact events for risk assessment and mitigation method development

WP1.3 follows closely the work of WP1.2, the development models and topological analysis algorithm in WP1.2 has been used to analyze the low-probability but high-impact events in the network, that is to assess the risk caused by intentional attacks on the power grid. Key vulnerable lines in the network have been identified, consequently, the method of mitigating the risks by enhancing the key lines can be adopted. The related technical details and associated publication are as aforementioned in above description of WP1.2.

WP1.4 Multi-objective optimization method for network design and expansion

The coordinated expansion planning method is proposed for the integrated gas and electrical power systems with bi-directional energy conversion. A bi-level multi-stage programming problem is established to minimize the investment and operational costs. A hybrid algorithm is proposed by combining the modified binary particle swarm optimization and the interior point method, which presents high computational efficiency in finding the optimized solution. Detailed contents are reported in Section 1.5.1.6. One journal paper and one conference paper published to describe the work.

Work Package 2 Efficient and reliable operation strategy for harmonized gas and electric energy distribution

WP2.1 Optimal energy flow model for energy system integrated with multi-carriers

WP2.1 proposes the energy flow models and formulate the optimal energy flow problem, considering network constraints, based on the work investigated in WP1.1 and WP1.2. The optimal energy flow in the integrated gas, heating and power system is studied. It is shown that the harmonized integration utilizes the flexibilities from heating and gas systems to help power systems to accommodate renewables. WP2.1 is closely related to WP2.2, the detailed contents of the two work tasks are described in Section 1.5.1.3 – 1.5.1.4. Two journal papers have been published to report the results.

WP2.2 Multi-time period optimization method for the integrated energy system

Following WP2.1's work, in this work task, the optimal operation of the integrated energy systems is further developed as a multi-time-period optimization problem by taking the different response times of the energy systems into account. For example, the transient gas flow and steady-state power flow are combined to formulate the dynamic optimal energy flow

in the integrated gas and power systems. Detailed contents are introduced in Section 1.5.1.3 – 1.5.1.4 as aforementioned. One journal paper and one conference paper have been published according to the results.

WP2.3 Coordinated control strategy to improve the reliability

Based on the optimization models built in the previous WPs, in WP2.3, the coordinated operation strategies for different devices across multiple energy carriers are developed, e.g., the coordination between linepack storage and battery energy storage to effectively utilize their capacities are investigated. The coordination of bi-directional energy conversions in gas and power systems are also studied. Detailed contents are reported in Section 1.5.1.5. Two journal papers and one conference paper have been published to report the work.

WP2.4 Online tool development for the integrated energy systems

In WP2.4, a stochastic optimization approach based on the approximate dynamic programming (ADP) for the multi-time-period optimal energy flow in integrated energy systems is proposed. The capability of ADP to deal with uncertainties is utilized while at the same time the real-time updated forecast information is utilised to adjust the day-ahead optimal schedule online. The simulation results demonstrated the effectiveness of the proposed algorithm. The technical details can be found in the conference paper attached in the annex entitled '*Hybrid approximate dynamic programming approach for dynamic optimal energy flow in the integrated gas and power systems'*. Two conference papers have been published.

The core parts of the online program including the models and mathematical algorithms are completely developed. Currently an easy access online interface is under implementation. The link to the online tool will be provided at the project website.

1.4.2 Project evolution and other relevant issues

The project of "Harmonized Integration of Gas, District Heating and Electric Systems (HIGHE)" has been conducted by a project team led by Department of Energy Technology (ET) at Aalborg University (AAU), including project partners, Department of Development and Planning at AAU, Department of Industrial Economics and Technology Management (IØT) at Norwegian University of Science and Technology (NTNU), and Ramboll at Denmark.

The start of the project was postponed due to the researcher recruitment process. However, the project plan including technical contents, budget and partners remained the same. The project had a revised period of staring on December 1st, 2014 and ending at November 30th, 2017. The project has been conducted smoothly, the regular project meetings were held at Aalborg University, in addition to all project partners, the representatives from Energinet.dk normally attend the project meetings and make valuable contributions, such as network information, practical operation experiences. Some project meetings with specific topics, such as gas network operation, thermal system operation, etc. were also organised at the gas department at Energinet.dk and Ramboll headquarter in Copenhagen.

The project has been conducted with good international cooperation, the international partner, IØT-NTNU, has made very good contributions with rich experience in the economics of energy systems. Furthermore, the project PhD researcher had a research visit stay at Integrated Systems Engineering and Electrical and Computer Engineering Departments, The Ohio State University, USA, which produced good results with high-quality journal papers.

There were some difficulties and risks expected at the beginning of the project, such as lack of available experience in operating the systems with huge difference in response time; possible non-technical factors in the optimization; the scalability of the proposed method etc. these problems have been appropriately dealt with by the project team with the support from the collaboration with industrial and research organizations, in particularly, Energient.dk.

The overall project has been implemented as planned in general, according to the milestones, while the algorithms and program for the software tool have been developed, and the online installation is being conducted for accessing. No significantly unexpected problems had been experienced.

1.5 Project results and dissemination of results

1.5.1 Main activities and technical results of the project

In Section 1.5.1, the technical details for major technical achievements are presented. The relationships between project objectives and the section where reporting the relevant technical contents are given in Table 1.

Table 1 The relationship between the project objectives and the section reporting the technical details.

WP1 System design and network expansion planning for the gas/electric coordinated systems	
Project objective 1: Develop models evaluating the techno-economic aspects of energy system with multiple energy carriers	**Section 1.5.1.1**
Project objective 2: Develop the network expansion model and topological analysis of integrated gas, heating/cooling and electric systems	**Section 1.5.1.2**
Project objective 3: Conduct the risk assessment for the network.	
Project objective 4: Propose the optimization method for system expansion planning	**Section 1.5.1.6**
WP2 Efficient and reliable operation strategy for harmonized gas and electric energy distribution	
Project objective 5: Develop models and algorithm for solving the optimal energy flows of the integrated gas, district heating and electric systems	**Section 1.5.1.3 ~ Section 1.5.1.4**
Project objective 6: Develop optimization method for coordinated operation of the integrated energy system with consideration of temporal spatial correlation	
Project objective 7: Propose emergency control strategies to impose the reliability and secure the energy supply.	**Section 1.5.1.5**
Project objective 8: Develop an online software tool for coordinated operation of the energy systems.	

1.5.1.1 Stochastic models of energy profiles for techno-economic evaluation

In the first part, a methodology to characterize the spatiotemporal correlation of multiple energy profiles is proposed. **This work is presented on 2015 IEEE Power Energy Society General Meeting entitled 'A hidden Markov model representing the spatial and temporal correlation of multiple wind farms.'** The full paper is attached in the annex.

The proposed method consists of following steps. First, a hierarchical clustering method based on self-organizing maps (SOMs) is adopted to categorize the similar spatial patterns. Then the hidden Markov model (HMM) is designed to describe the temporal correlations among these joint states. Unlike the conventional Markov chain used to model the time series of a single wind farm, multiple time series of wind power at different locations is modeled. The proposed statistical modelling framework is compatible with the sequential power system reliability analysis. A case study on optimal sizing and location of fast-response regulation sources is presented. An illustrative diagram of the main idea can be seen in Fig. 2.

In this work, the productions of multiple wind farms are studied as the example. One-year hourly wind speed from 12 measurement sites in Denmark is collected. The geographical locations of these measurement site are marked in red in Fig. 3. The wind speed measurements are collected by the Iowa Environmental Mesonet (IEM). The hourly wind speed measurements are converted to power generation using the generic power curve of the wind turbines. The raw wind speed data and converted wind power are illustrated with the box-plot in Fig. 4.

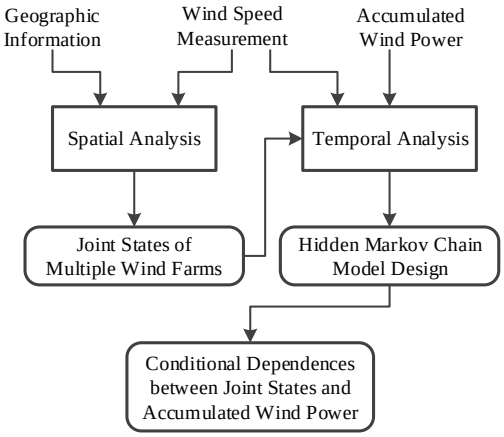

Fig. 2 Conceptual framework of wind power modeling for multiple wind farms

Fig. 3 Geographical locations of wind measurement points: the red markers show the wind power with complete 1-year data and used in this work

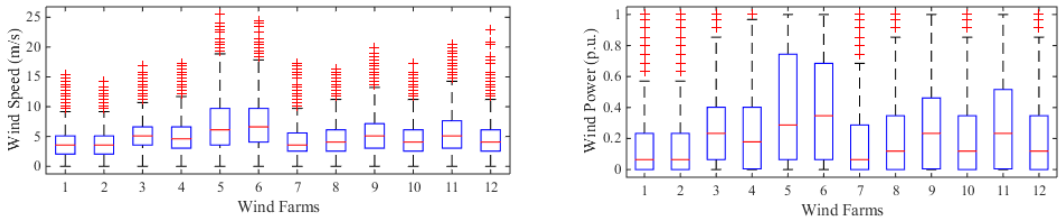

(a) Wind speed distribution (b) Wind power distribution

Fig. 4 Wind speed and wind power.

Self-Organizing Map

In the former studies, the multi-state wind generation models are usually used by dividing the wind power into several regions. However, these n-state models (typically $n = 3, 5, 7, 9$) are only for a single wind farm. In this work, we intend to build the joint states according to the power outputs from multiple wind farms. Let vector $\boldsymbol{P}(t) = [P_1(t),\ P_2(t),\ \cdots,\ P_N(t)]$ represent the wind power from N assumed wind farms at time t. And we use the Euclidean distance between $\boldsymbol{P}(t_i)$ and $\boldsymbol{P}(t_j)$ to quantify the similarity of these two wind power outputs at time t_i and t_j. The output vectors $\boldsymbol{P}(t)$ with similar pattern are categorized into the same joint state of the wind farms.

To find out the joint states, a hierarchical clustering method based on the SOM is employed. The SOM is a popular neural network proposed by *T. Kohonen* applied in classification and visualization. It is an unsupervised learning approach that projects and visualizes high dimension feature space onto a low dimensional lattice of weighted neurons [16]. The weight vector for each neuron on the lattice has the same dimension with the input vector $\boldsymbol{P}(t)$. Basically, there are 3 steps in the SOM based clustering, namely, the initialization, network tuning and clustering as the following.

1) Initialize the SOM Neuron Network. There are two categories of methods to initialize the SOM neuron network: the linear initialization approaches and the random approaches. Through Monte-Carlo simulation, we found that, in our case, the random initialization turns out to be effective and has little influence on the clustering results. Besides the initial weights of the

neurons, the initial parameters including the learning rates, the total number of iteration and the neighborhood function, will also be set up. In the project, the hexagonal pattern of the neuron network positions is applied. The weights of the neurons are initiated randomly. The total number of iteration is set to 500, and the Gaussian neighborhood function is used.

Fig. 5 illustrates the size of the SOM associated with the quantified clustering errors (QCE) measured by the average distance between each data vector and its clustering center. This helps to select the size of the SOM with the tradeoff between computational burden brought by the increasing cluster number and clustering accuracy. It can be seen from Fig. 5 that if there are more than 300 neurons, the QCE decreases slowly. So the size of the SOM is selected as 300 neurons.

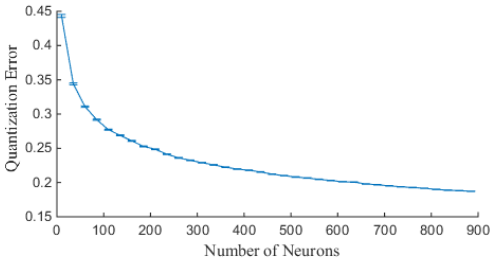

Fig. 5 The quantification of clustering errors

2) Tune the SOM Neuron Network. After the initialization and parameter setting, an iterative process is conducted to train the SOM neuron network. The training is divided into a rough training stage and a fine tuning stage. First, at the rough training stage, the learning rates and the neighborhood radius decreases radically. At the fine-tuning stage, these 2 parameters are adjusted more smoothly so that the network is tuned slowly.

During each iteration process, the generations of the assumed wind farms $\boldsymbol{P}(t)$ at a randomly selected hour t will be the input of the SOM. A best matching unit (BMU) will be found among all the neurons. The BMU has a weight vector which is closest to the current input. Before updating the weights of the neurons, a kernel function $H(\sigma)$ and training rate η will be updated. In the kernel function, σ refers to the pre-defined size of the neighborhood neurons determined by the Euclidean radius around the BMU. During the training process, the learning rate η will be slightly decreased to refine the speed of tuning. The weights of the neurons W will be modified according to the following equation:

$$\begin{aligned} W_{ij}(t+1) &= W_{ij}(t) + \Delta W_{ij} \\ \Delta W_{ij} &= \eta(t) H(\sigma)\ \ X_s(t) - W_{ij}(t) \end{aligned} \tag{1}$$

where $X_s(t)$ is the current sample at the tth iteration and $W_{ij}(t)$ is the weight vector of the neuron on the ith row and the jth column of the neuron on the lattice. From (1) one can see that the update of neurons' weight depends not only on the learning rate $\eta(t)$ but also on $H(\sigma)$.

3) Cluster the SOM neurons on the lattice. Fig. 6 illustrates the results of the clustering. A SOM with total 299 (13×23) neurons is built. The distances between the neurons are illustrated in Fig. 6(a). The darker color of the hexagon indicates the larger distance between the neurons. Then those neurons that are far from each other are classified into different clusters while those are close to each other are in the same cluster. Fig. 6(b) shows the final clusters with different colors on the SOM lattice.

Here in the second cluster layer, the problem to choose an appropriate cluster number still exists. In order to find the right number of clusters, the Davies-Bouldin index (DBI) is used to quantify how well the clustering is classified. DBI is a systematical measurement involving two kinds of distances: one is the QCE used before to select the SOM size, and the other is the distances between the cluster centers. An ideal cluster of data is to make the QCE as small as possible while the distances between the cluster centers as large as possible. This ensures that those $\boldsymbol{P}(t)$ vectors with similar patterns are put into the same cluster, while those irrelevant ones are in different clusters.

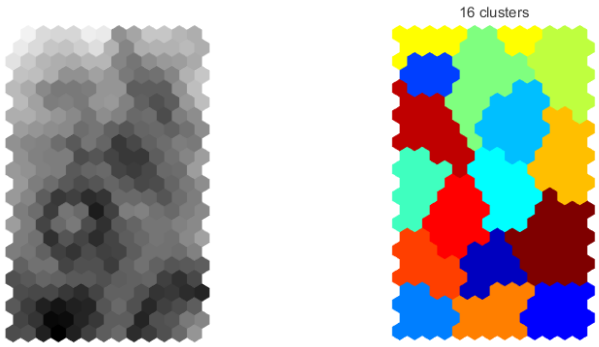

(a) Distance matrix (b) Cluster of SOM map units

Fig. 6 The hierarchical clustering of wind power outputs of multiple wind sites.

The Hidden Markov Chain Model

After the joint states for multiple wind farms are found. The next step is to figure out the statistic independencies between these states. Unlike the conventional Markov chain model, hidden Markov model (HMM) is used in this work. It enables us to characterize the relationship between the total generation of several wind farms and the output of each wind farm.

Fig. 7 shows the general architecture of an instantiated HMM. Each oval shape represents a combined state of several wind farms clustered in the previous section. In Fig. 7, the rectangle shape represents the total power output of these wind farms. In this diagram, the random variable $x(t)$ ($x(t) \in \{x_1, x_2, x_3, \cdots\}$) is the hidden state at time t. $x_1, x_2, x_3, \cdots$ are the joint states clustered in the previous section. The random variable $y(t)$ is the observation at time t with $y(t) \in \{y_1, y_2, y_3, \cdots\}$. The arrows in the diagram denote conditional dependencies and the probabilities.

The parameters of the HMM are of two types, transition probabilities P_{sij} and emission probabilities P_{eik}. The transition probabilities P_{sij} control the way the hidden state at time t is chosen with the given state at time $t-1$. The emission probabilities P_{eik} represents the probability of y_k comes from the state x_i at time t. It is worth noting that according to the property of Markov chain, the state $x(t)$ depends only on the past state $x(t-1)$, while the state at time $t-2$ and before have no influence. Similarly, the value of the observed variable $y(t)$ only depends on the value of the hidden variable $x(t)$. Assuming that there are X_N states and Y_M observations, let the matrices $A = [P_{sij}]_{X_N \times X_N}$ and $B = [P_{eik}]_{X_N \times Y_M}$ be the transition matrix and emission matrix, respectively. The aggregated wind power is divided into 9 states in this work. Hence $X_N = 16$ and $Y_M = 9$. An HMM can be denoted as

$$\lambda = (\pi, A, B) \tag{2}$$

Here π refers to the initial condition probability vector of the HMM. There are 3 key algorithms developed for an HMM implemented in applications, namely Forward- Backward algorithm, *Viterbi* algorithm and *Baum-Welch* algorithm. Their roles are introduced as following.

1) *Baum–Welch* Algorithm: Given an observed value series $\boldsymbol{y} = [y(t_1), y(t_2), \cdots, y(t_T)]$ and state series $\boldsymbol{x} = [x(t_1), x(t_2), \cdots, x(t_T)]$, an HMM will be calculated including the matrices A and B to achieve the maximum $P(\boldsymbol{y}|\lambda)$.
With the *Baum–Welch* Algorithm, we can build the HMM according to the joint states of multiple wind farms and the aggregated wind power. First, we use high dimensional clustering algorithms such as SOM to build the joint states of multiple wind farms. A time sequence of the joint states $\boldsymbol{x}$ then can be obtained. The observation series $\boldsymbol{y}$ can be easily acquired from the aggregated generation. Given the two time sequences $\boldsymbol{x}$ and $\boldsymbol{y}$, the HMM matrices A and B can be trained. The joint states consist of the information on spatial correlation, and the Markov chain model consists of the information on the temporal correlation of the wind farms.

2) Forward-Backward Algorithm: Given an observed value series $\boldsymbol{y} = [y(t_1), y(t_2), \cdots, y(t_T)]$ and an HMM $\lambda = (\pi, A, B)$, $P(\boldsymbol{y}|\lambda)$ denoting the probability that model λ generates series $\boldsymbol{y}$ will be calculated**.**

With the *Forward-Backward Algorithm*, the probability of the generated time series can be calculated. For a power system with multiple wind farms, with the given HMM, the probability of a certain output state sequence $\boldsymbol{y}$ can be obtained. Though it is out of the scope of this project, this algorithm can still be used in the wind power forecasting.

3) Viterbi Algorithm: Given an observed value series $\boldsymbol{y} = [y(t_1), y(t_2), \cdots, y(t_T)]$ and an HMM $\lambda = (\pi, A, B)$, a most likely state series $\boldsymbol{x} = [x(t_1), x(t_2), \cdots, x(t_T)]$ will be generated to achieve the maximum $P(\boldsymbol{y}|\lambda)$.

If the aggregated wind power is acquired, with *Viterbi* Algorithm, we can generate the wind power time series for each wind farm. Sometimes the historical data for the individual wind farm is not so easy to access. The system operators provide only the total wind power. With the trained HMM and *Viterbi* algorithm, it is possible to generate the individual wind farm data reasonably.

Fig. 8 shows both the state transition probabilities and emission probabilities from the states to the observations. In these figures, each block in the ith row and jth column shows the element in the matrices $[P_{sij}]$ and $[P_{eik}]$, respectively. The darker color indicates a higher probability in these figures.

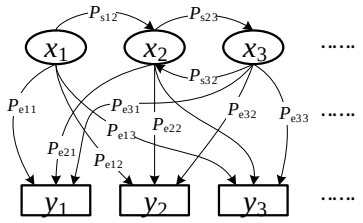

Fig. 7 An example of hidden Markov model.

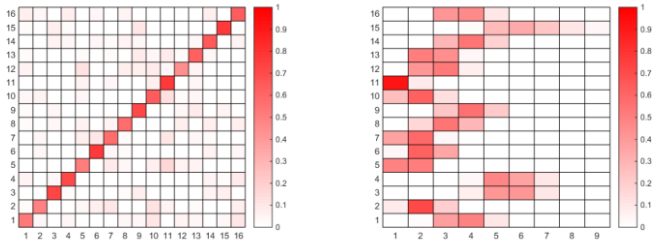

(a) The state transition matrix (b) The emission matrix

Fig. 8 The hidden Markov model for multiple wind sites in Denmark.

1.5.1.2 Network models and risk assessment of future expended energy system

The 2nd highlighted achievement of this project is the topological analysis of the power system. Among different energy networks including heating, gas, and electricity, the power grid has the most complex topology. So in this project, a maximum flow based complex network approach to identify the critical lines in a system is proposed. **This work is published on IEEE Transactions on Smart Grid entitled 'Power system structural vulnerability assessment based on an improved maximum flow approach.'** The full paper is attached in the annex.

The proposed method consists of two major steps. First, the power network is modeled as a graph with edges (transmission lines, transformers, etc.) and nodes (buses, substations, etc.). The critical scenarios are identified by using the principal component analysis (PCA) and convex hull. Then the second step is to use an improved maximum flow based complex network (CN) approach for topology analysis. Weighted vertices in the network are considered, enabling considering the selected operating conditions when identifying the vulnerable lines. The proposed method is validated using the western Danish power system. The vulnerable lines in the network are ranked. Simulation results demonstrate the effectiveness of the method by intentional attacks and comparison with the planning strategy from the system operator. To

validate the proposed method, comparative studies with the existing method has been conducted in western Danish power system.

Graph model of the energy networks for topological analysis

A power system can be considered to be a large complex network with vertices and edges. In a power system, the buses with the generators and loads can be identified as the vertices in the network, and the transmission lines can be considered as the edges or links. Supposing the network is represented as a graph $G = (V, E)$ with n vertices in set V and k edges in set E. Then the adjacency matrix A is to define the connectivity of the graph. The elements of the adjacency matrix, aij, denote the weights for the edge connecting the two nodes. $a_{ij} > 0$ means that there is a connection between node i and node j while $a_{ij} = 0$ if there is no connection between i and j. The capacities of the transmission lines are selected as the edge weight in constructing the network in this study.

Besides the edge weight, the vertex weight is also utilized in modelling the power system with a graph. In a power system, generators (or loads) at different buses would inject (or extract) different amount of power to (or from) the system, and thus, it will influence the vulnerability assessment results even if the edges are the same. In this work, the vertices with net generation are defined as source nodes in the graph, while those with net consumption are defined as sink nodes. The vertices in this paper are those substations. And the net generations or consumptions of the source or sink vertices are used as the weights for these vertices, i.e. the power flows out (positive weights) or into (negative weights) the vertices.

With the graph model for the topological analysis of the power grid is built, the maximum flow based method for power system structural vulnerability assessment is proposed. The vulnerability is defined as a measure of net-ability, path redundancy and survivability of the grid. A bus or a line is vulnerable if its removal has a significant impact on the network efficiency, redundancy, and robustness to failures.

The maximum flow problem is a classical optimization problem in CN theory. In a graph $G(V, E)$, let $s, t \in V$ be the source and sink nodes of G, respectively. And the edge capacity c_{uv} represents the maximum amount of flow that can pass through the edge between vertex u to vertex v. Fig. 9 illustrates an example of the maximum flow. In this graph, there are 10 vertices. Node 1 and node 2 are the source nodes, while node 8, 9 and 10 are the sink nodes. In Fig. 9(a), the capacities are marked on the edges. Fig. 9(b) gives the feasible maximum flow from node 1 to node 8. On the edges, the possible flow is marked. From this figure, we can see that the edges $(4,8)$ and edge $(5,7)$ reach their limits while other lines are not fully made use of. The value of the maximum flow is calculated as 8 in this case.

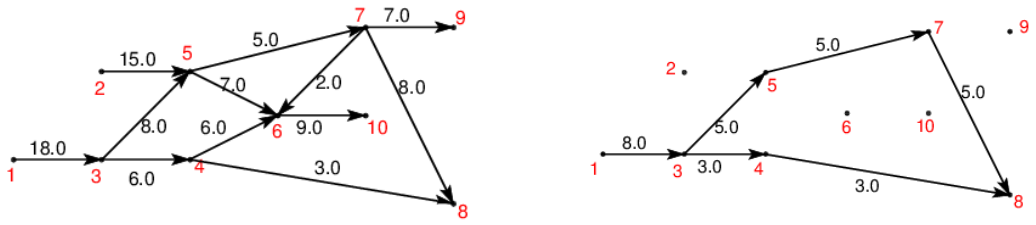

Fig. 9 The maximum flow of the graph (the node is numbered in red). (a) The graph topology with capacity constraints. The edge capacities are marked with black numbers. (b) A maximum flow from vertex 1 to 8. The flow through the edges are marked with black numbers

There is a major concern that only the constraints on the edges, i.e., the capacity of the transmission lines, are taken into account in the existing work. In real power systems, however, the generators also have their capacity limits. It could not be ignored if the capacity of the generation at the source nodes is less than the maximum flow. Another drawback is

that the specific pair of source and sink nodes should be determined before calculating the max flow. This means that if the system has N source nodes and M sink nodes, the maximum flow has to be calculated for $N \times M$ times. For example Fig. 9(b) illustrates only the max flow from node 1 to node 8. By picking up this pair of source and sink nodes, it is assumed that the load at node 8 can be supplied and only supplied by the generation at node 1. Meanwhile, by summarizing multiple maximum flow between different source-sink pairs, it is likely to find some flows to violate the capacity constraints.

Improved maximal flow approach for vulnerability assessment

To encounter the multi-source multi-sink problems, the modified max flow problem is employed in this task. First, the vertex weight is taken into account by adding a virtual node connected to each source and sink node. For the source nodes, the direction of the virtual link is always from the virtual source node to the real source node. While for the sink nodes, the direction of the virtual link is always from the real sink node to the virtual sink node.

Second, for those complex power grids with multiple source nodes and sink nodes, two more nodes are added to the graph, namely the consolidated source or sink. One node connects with all the virtual source nodes while the other connects to all the virtual sink nodes. The weights for the edges added here are all set to infinite. We use these virtual nodes with extremely large weights to summarize all the source nodes and sink nodes, respectively.

The modern power systems are more and more interconnected, particularly in Europe. The cross-border energy exchange provides the national power systems with flexibility and reliability. In this project, if the studied power system has interconnections with neighboring grids, a single node is used to equivalently represent each neighboring system, respectively. This brings a new problem that it is not easy to identify whether these equivalent nodes are source nodes or sink nodes because they represent the whole areas of the power systems, and the flows into or out of these nodes are hard to be quantified. Hence in this project, we make use of the historical data for the vertex weights of these equivalent nodes. Multiple scenarios are evaluated considering the variations of the import/export power.

Based on the max flow calculated, the centrality index is adopted to rank the importance of the lines. The centrality of a network refers to the portion of flow passing through a specific edge in a network. In the existing work, the components with higher centrality in the graph have more influence on the network properties, and hence more vulnerable in the system. The centrality index is defined as

$$C_{ij} = \sum_{u=1}^{M} \sum_{v=1}^{N} f_{ij}^{uv} \tag{3}$$

where f_{ij}^{uv} is the flow passing through the edge between node i and node j. u and v are the source and sink nodes. Since the multi-source multi-sink maximum flow is converted to the single-source single-sink one, we can get rid of the subscripts of source node u and sink node v. Instead, s is used to denote the sth scenario. Under this scenario, the maximum flow of the whole network is $f_{max}^{(s)}$. Let $f_{ij}^{(s)}$ be the flow passing through the branch ij under the maximal flow condition. The centrality index is

$$C_{ij}^{*} = \sum_{s=1}^{n} f_{ij}^{(s)} \tag{4}$$

And C_{ij}^{*} is then normalized by the maximum flow $f_{max}^{(s)}$ under the sth scenario.

Although the modified max flow problem with vertex weight enables taking the different scenarios into consideration, the computational burden rises with the number of addressed scenarios, i.e. operating conditions of power systems. In this work, the critical scenarios are selected from the historical operation data. The basic idea is to use the convex hull or convex envelope to pick out those scenarios in which some components may approach the limits of their capacities. Here we use a vector $\boldsymbol{V}(t) = [P_1(t), P_2(t), \ldots, P_n(t)]^T$ to denote an operating

condition at time t, where P_i is the active power at bus i. The bus is a generation bus when $P_i > 0$, while it is a load bus when $P_i < 0$. Within the time horizon of interest $0 \sim T$, there could be many $\boldsymbol{V}(t)$s in the nth-dimensional space. The convex hull of set $S = \{\boldsymbol{V}(t), t \in [0,T]\}$ is the smallest convex set that contains all the $\boldsymbol{V}(t)$s in S. And the operating conditions on the convex hull are the extreme operating scenarios. Take 2-dimensional plane for example. Supposing that there are a lot of points in the plane, the convex hull of these points can be imagined as the shape formed by a rubber band stretched around these points. But for the case in this work, the convex hull in the nth-dimensional space could be very complex and impossible to be visualized. Hence, a reduction method is needed to transfer the high-dimensional vector into a low-dimensional space.

In order to reduce the dimensions of the data, the principal component analysis (PCA) method is employed. The PCA is a statistical method for pattern recognition. It consists of two steps: the first is the orthogonal transformation to convert a set of observations of possibly correlated variables into a set of values of linearly uncorrelated variables; the second step is to select the proper dimensions in the newly created spaces with the desired integrity of data, i.e., linear coordinate transformation and dimension selection. The orthogonal transformation is linear and is used to transform the data into a new coordinate system so that the largest variance of the data lies on the first coordinate; the second largest variance lies on the second coordinate, and so on. Mathematically, the transformation is defined by a set of n-dimensional row vector of weights $\boldsymbol{w}_k = [w_{1k}, w_{2k}, \dots, w_{nk}]^T$. For each variable in the new coordinate, $P_{Tk}(t) = \boldsymbol{w}_k \cdot \boldsymbol{V}(t)$, which comprise the new space $\boldsymbol{V}_T(t) = [P_{T1}, P_{T2}, \dots, P_{Tn}]^T$.

From the previous sections, we have proposed a systematical method for power system vulnerability assessment. The method helps the system operators to gain as much information as possible from both power grid structure and historical operation data. The complete procedure of the proposed method can be summarized as follows.

Step 1. Obtain the power system structure with capacities of the transmission lines, generator capacities and loads. Formulate the network model.
Step 2. Perform PCA on the historical data and project the data in a low (typically 2) dimensional space. Select the scenarios according to the convex hull.
Step 3. Weight the vertices with the selected scenarios and make network modifications.
Step 4. Compute the max flows of the network with the selected scenarios and summarize the centralities of the lines based on the centrality indices.
Step 5. Check the ranking of the importance of the lines by examining the remaining max flow with the residue network where each of critical lines is removed respectively.

Case study on the western Danish power system

In this project, the Danish power system is used as the case study to demonstrate the proposed method, as shown in Fig. 10. The Danish power system is divided into two asynchronous parts, the western part (DKW system) and the eastern part of the system (DKE system). The graph shows the practical system topology of 2010 DKW system. The 400 kV, 150 kV and the 60 kV voltage levels are included in the simulation while the 60 kV system is not illustrated in the figures.

In Europe, the cross-border interconnections play an essential role in enhancing the overall system flexibility and reliability, especially with a high penetration level of wind power. The studied DKW system has a series of international connections with neighboring countries and the DKE system. In the north, there are several HVDC tie-lines connected with Sweden and Norway and more links are under planning. The DKW and DKE power systems are interconnected by an undersea HVDC link. There are several AC tie lines synchronizing the DKW system with the northern German/European power system. Geographically, we can see that DKW power system act as the transmission corridor connecting Norway, Sweden, Germany and DKE system. Hence the power systems in Norway, Germany, Sweden and DKE

can be represented by the equivalent nodes. According to the operational data from Energinet.dk, the offshore wind farm has significant impacts in DKW system, which mainly comes from large wind farms such as Horns Rev located on the western coast of Denmark. So it is also considered as an equivalent node.

Fig. 11 illustrates the operational data from the year of 2011 with the box plot. It shows the variation of the vertex weights for the equivalent nodes. The bottom and top of the box are always the first and third quartiles of each data set, denoted as q_1 and q_3, respectively. Points are drawn as outliers with the red cross if they are larger than $q_3 + 1.5(q_3 - q_1)$ or smaller than $q_1 - 1.5(q_3 - q_1)$. From this figure, we can further demonstrate that the DKW system is a transmission corridor connecting its neighboring power systems. The physical exchange between DKW system and Norway, Sweden and Germany can usually reach 1000 MW, while the total demand within the system can be only up to 3500 MW. Hence, it is necessary to consider the time-vary vertex weights for those equivalent nodes around DKW system. Compared to these equivalent nodes, those nodes inside the DKW system have much fewer variations. So their weights are fixed with one typical operating condition.

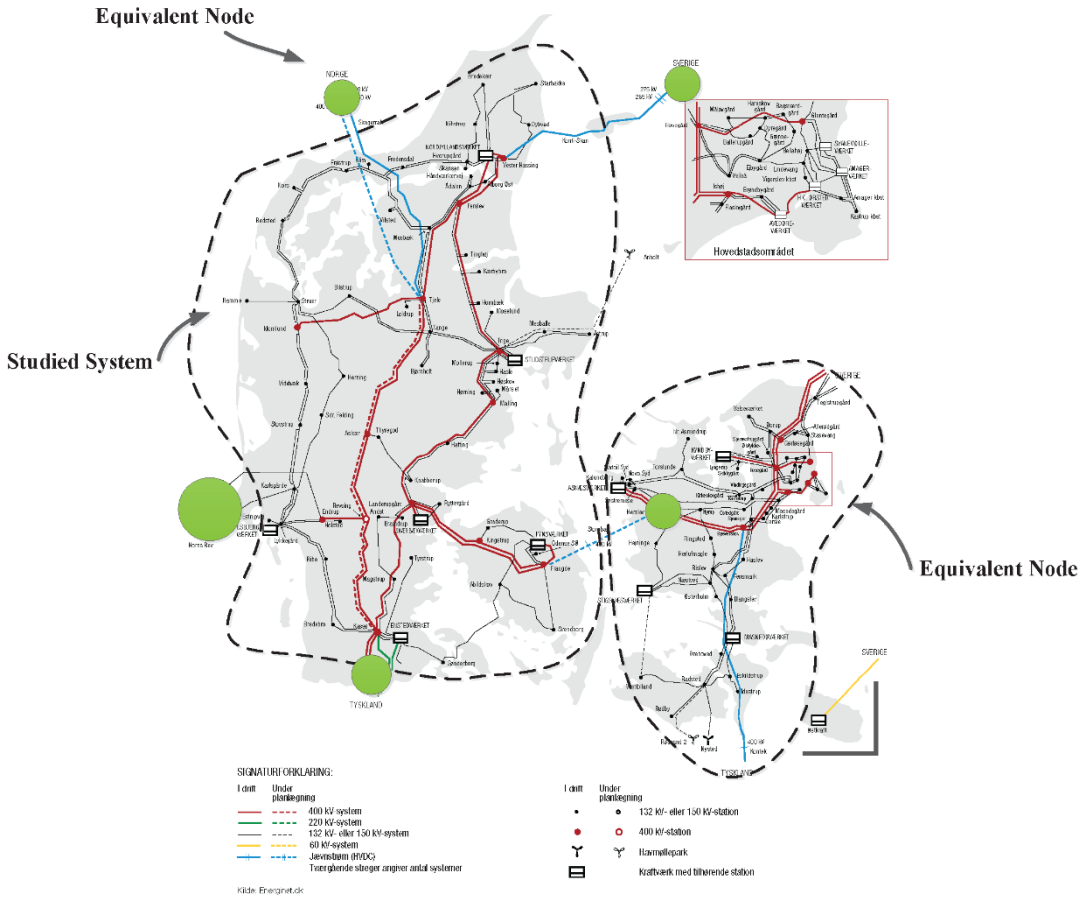

Fig. 10 The power system in Denmark

With the historical data collected, the PCA is performed to project the variables in Fig. 11 to a low dimensional space. After the PCA, it is much easier to select the studied scenarios of interest. Fig. 12 uses the convex hull in the 2-D PCA plot to mark the extreme scenarios in 2010. 13 of 8760 operating conditions are selected, as shown in Table 2. The PRM and LOC refer to the power production from the central power plants and distributed generators, respectively. Within these extreme scenarios, the transmission capacities of corresponding lines have been reached. For example, in case 4 and 6, the physical exchange between DKW and Norway has reached the maximum value. Also in case 12, the generation of offshore wind farm takes up to 45.5% of total load in DKW system.

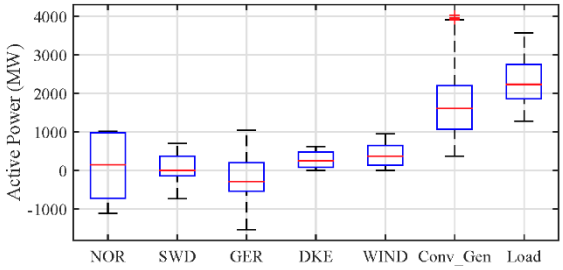

Fig. 11 The power variation on the cross boarder transmission lines and wind farms

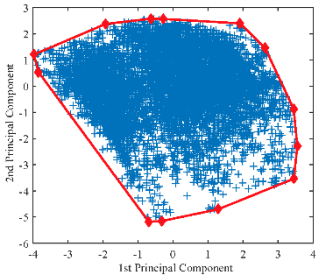

Fig. 12 Convex hull based selection of the extreme scenarios

Table 2 The extreme operating conditions associated with DKW system

No.	Date	Hour	NOR	SWD	GER	DKW-DKE	DKW-WIND	PRM	LOC	Load
1	'01-18-2011'	2	-957.4	-126.9	931.5	-567.9	471.2	730.3	567.8	1973.4
2	'04-30-2011'	14	-934.5	104.3	923.9	-573.8	238.1	670.2	371.9	2016.8
3	'04-28-2011'	3	-524.6	455.6	58	-595.5	495	633.9	178.9	1689.6
4	'04-14-2011'	21	1004	208	-1511.6	-588.3	14.9	1497.3	695.2	2425.9
5	'06-29-2011'	9	995.6	680.9	-1300.3	-401.2	109.1	1101.4	681.1	2741.5
6	'04-20-2011'	20	1005	679.5	-1522.3	-160.2	34.5	1562	409.5	2226.9
7	'06-04-2011'	12	991.5	680.2	-1434.2	505.7	21.9	1739.6	546.5	2005.6
8	'07-01-2011'	10	989.2	680.9	-1418.6	527.4	706.5	1032.3	599.6	2765.2
9	'11-25-2011'	8	733.2	-9.9	-808.6	566.5	755	836.3	524.4	3060.8
10	'11-25-2011'	9	734.6	-180.3	-733.8	591.2	797	995.6	593.3	3173.8
11	'12-08-2011'	19	408.3	-710	-499.4	591.6	789.1	1447	717.1	3301.4
12	'11-27-2011'	7	-959.3	-733.6	758.7	578	822.2	603	245.1	1806.3
13	'04-05-2011'	17	-958	-735.9	942	453.4	679.4	1149.1	769.3	2788.4

With the identified critical scenarios, we compare the centrality indices computed by two different max-flow-based approaches. The criticality of a line can be evaluated in terms of the value of the centrality indices. The centralities are normalized by the max flow value of each scenario. The centralities $\overline{C_{ij}^{*}}$ of the lines using the proposed method are calculated. Fig. 13 illustrates the result with geographical information. The most vulnerable lines are the transmission corridor between Norway and Germany, consisting of the HVDC lines and 400 kV line intersecting Denmark from the north to the south. These lines are the most important transmission corridor between Norway and Germany. As shown in Fig. 10, the dashed lines mean that double-circuit lines were planned in 2010. The computation result is consistent with the system operator's network planning strategy, which is obtained by very experienced staff with numerous simulations. Other vulnerable lines marked red here is another 400 kV transmission corridor along with the east coast of Denmark, connecting Sweden and Eastern Danish power systems.

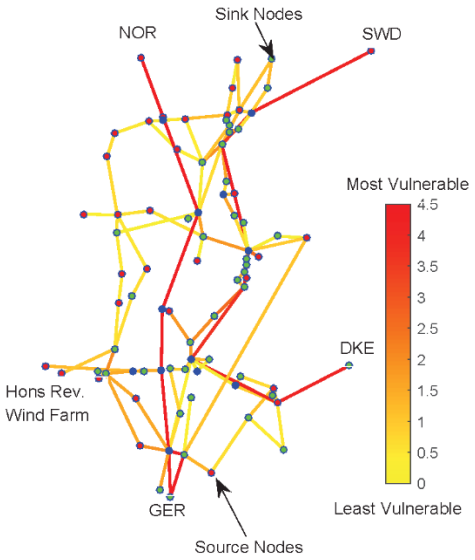

Fig. 13 Assessment of the vulnerable lines in DKW system considering vertex weight

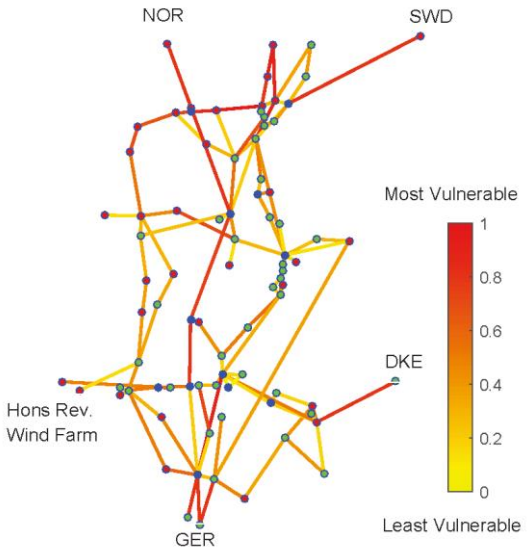

Fig. 14 The vulnerable lines in DKW system with the conventional max-flow method

We further compare the proposed method by investigating the effect of intentional attacks on the lines ranked by the method from existing method and random attacks. 40 lines are selected and removed from the DKW system sequentially, and the remaining maximum flow for the residue system is calculated in each removal step. The results are illustrated in Fig. 15.

In Fig. 16, the remaining load is calculated following the 3 attack patterns as the same as Fig. 15. At each simulation step when the line is removed, an AC optimal power flow (ACOPF) is calculated using DigSilent/PowerFactory. The objective of the ACOPF is set as minimum load shedding. The constraints include the AC power flow equations, bus voltages, line capacities, generators' maximum active and reactive power, etc. In this numerical experiment, 180 lines are removed eventually, resulting in nearly 80% load unsupplied with the intentional attacks. This simulation experiment indicates the same conclusion with Fig. 15, but this numerical simulation is more from the topological point. From physical system's perspective, Fig. 16 shows that the remaining load in the system decreases more quickly with the removal of the lines ranked by the improved max-flow based centrality index. This indicates that the system is more sensitive to the critical lines identified by the proposed method.

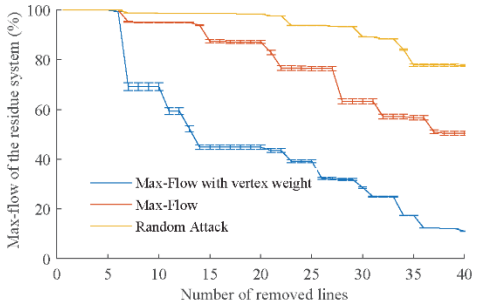

Fig. 15 The comparative study on the removal of lines.

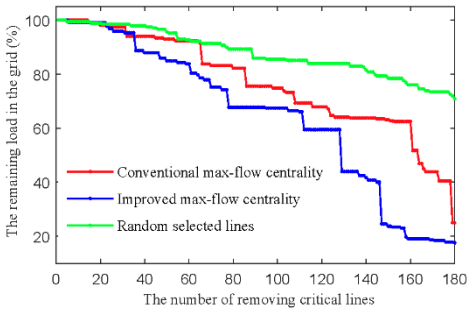

Fig. 16 The remaining load under different removal strategies.

It can be seen from simulation results that compared to the conventional methods; the vertex weights are taken into account. And the superposition of the max-flow of each generation-consumption pair is replaced by an all-together calculation method. The ranks of the line vulnerability obtained from the proposed method show better consistency with the system operator's planning strategy than that obtained from the existing method. Furthermore, the superiority of the proposed method in identifying the critical lines is verified by a series of simulated system attacks (i.e., line removal from the system). The proposed method provides an alternative way for power system vulnerability assessment and it could be a complementary

tool to the existing electrical engineering tools for the vulnerability analysis in system planning. The critical lines identified according to this topological model should be enhanced to mitigate the risks in energy networks.

1.5.1.3 Multi-time period optimal energy flow for harmonized gas and electric energy distribution

In addition to the modeling of the energy profiles and networks, the energy flows in gas and heating systems is analyzed in Section 1.5.1.3 to 1.5.1.4. Rather than being dependent, the energy flow models are integrated with the load flow in power systems. In this part, the quasi-steady-state gas flow is combined with the power flow so that the compressible feature of natural gas can be considered. The power-to-gas technology is also modeled together with gas-fired generators to enable bi-directional energy conversion between the gas and power systems. The major advance of the proposed model is that the linepack storage in every pipe can be assessed and optimally utilized. **This work is published on IEEE Transactions on Sustainable Energy entitled 'Dynamic optimal energy flow in the integrated natural gas and electrical power systems'.** The full paper is attached in the annex.

Fluid dynamics for the gas flow

The natural gas flow is driven by the pressure along the pipelines in correspondence to its ingredient density, temperature, pressure, etc. The gas states such as velocity, temperature, density, pressure, etc. can be linked by the one-dimensional fluid dynamics along the pipe. This process can be described using 3 major equations: the momentum equation, the material-balance equation and the state equation. The momentum equation, also known as Navier-Stokes equation, describes the momentum transport in the continuum of natural gas. The equation takes the following form.

$$\frac{\partial(\rho\omega)}{\partial t}+\frac{\partial(\rho\omega^2)}{\partial x}+\frac{\partial p}{\partial x}+g\left(\rho-\rho_a\right)\sin\alpha+\frac{\lambda}{d}\frac{\omega^2}{2}\rho=0 \tag{5}$$

ρ, ω and p are the gas density, flow velocity and pressure, respectively. There are 5 terms in (5). The first 3 terms describe the acceleration, convective, hydrostatic effects of the natural gas. The 4th term is associated with the altitude deviation of the pipe. The 5th term represents the second-order deviatoric stress tensor.

The material-balance equation expresses the conservation of the mass in the gas pipeline as follows.

$$\frac{\partial\rho}{\partial t}+\frac{\partial(\rho\omega)}{\partial x}=0 \tag{6}$$

The state equation links the gas temperature, density, and pressure. It has various forms. For example, the ideal gas law indicates $PV=nRT$ but it only works for natural gas at less than 1 MPa and 20 ℃. Other forms, including the van der Waals equation, the Benedict-Webb-Rubin equation, etc. improve the modeling accuracy for real gas systems. This work adopts a simple relationship between the pressure and density using the sound speed in gas $c=\sqrt{ZRT}$, where Z is the gas compressibility factor.

$$p=c^2\rho \tag{7}$$

Using the fluid dynamics to describe the energy transmission in the gas pipelines is rather complex. The assumptions are made to simplify the aforementioned momentum equation (5) and the material-balance equation (6) so that the network constraints can be formulated accordingly.

The first assumption is that the gas transmission is isothermal, which means that the gas temperature is assumed to be constant. Neglecting the temperature variation, T is a constant. Consequently, c^2 in (7) becomes constant. And it is assumed that the altitude does not change along the pipes, which leads to $\alpha=0$, then (5) becomes

$$\frac{\partial\ \rho\omega}{\partial t}+\frac{\partial p}{\partial x}+\frac{\lambda}{d}\frac{\omega^2}{2}\rho=0 \tag{8}$$

The mass flow rate has the similar meaning to the gas velocity ω in representing the amount of the gas flow. It has the following relationship with the gas density.

$$M=\rho wA \tag{9}$$

Using the mass flow rate to replace the gas velocity ω, then (6) and (8) become

$$\frac{\partial\rho}{\partial t}+\frac{\partial M}{A\partial x}=0 \tag{10}$$

$$\frac{\partial M}{A\partial t}+\frac{\partial p}{\partial x}+\frac{\lambda}{2d}\frac{M^2}{\rho A^2}=0 \tag{11}$$

Differencing the partial differential equations

After the partial differential equations describing the gas fluid is simplified, they are turned into their differencing form. In this project, the following *Wendroff* difference form is used to approximate the solutions to the partial differential equations (10) and (11).

$$\begin{cases}\dfrac{\partial X}{\partial t}\approx\dfrac{1}{2}\left(\dfrac{X_{i+1,t+1}-X_{i+1,t}}{\Delta t}+\dfrac{X_{i,t+1}-X_{i,t}}{\Delta t}\right)\\ \dfrac{\partial X}{\partial x}\approx\dfrac{1}{2}\left(\dfrac{X_{i+1,t+1}-X_{i,t+1}}{\Delta x}+\dfrac{X_{i+1,t}-X_{i,t}}{\Delta x}\right)\\ X\approx\dfrac{1}{4}\ X_{i+1,t+1}+X_{i,t+1}+X_{i+1,t}+X_{i,t}\end{cases} \tag{12}$$

where Δt and Δx indicate the time step and the spatial step respectively. The *Wendrof* differencing form has 2nd order accuracy with the truncation error $O(\Delta t^2+\Delta x^2)$. The differencing scheme is shown in Fig. 17.

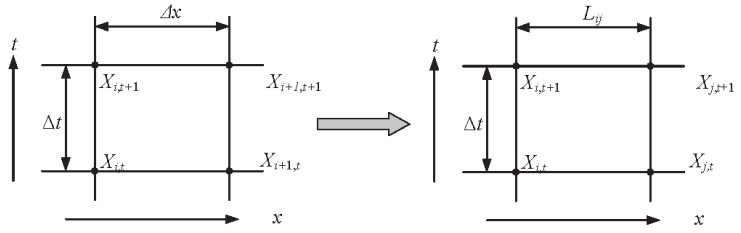

Fig. 17 Finite difference cells.

With the differencing scheme, the pipeline is divided into several segments. And for every segment of the pipeline with length Δx, momentum and material-balance equations apply. In this work, a variable spatial step Δx is used. The observation points are set at the two ends of the pipe i,j. So $i+1$ is replaced by the other end of the pipe j and Δx is replaced by the length of the pipe L_{ij} in (12). Then for every pipe ij, (10), (11) can be replaced by (13) and (14)

$$\rho_{j,t+1}+\rho_{i,t+1}-\rho_{j,t}-\rho_{i,t}+\frac{\Delta t}{L_{ij}A_{ij}}\left[M_{j,t+1}-M_{i,t+1}+M_{j,t}-M_{i,t}\right]=0 \tag{13}$$

$$\begin{aligned}\frac{1}{A_{ij}}\ M_{j,t+1}+M_{i,t+1}-M_{j,t}-M_{i,t}\ &+\frac{\Delta t}{L_{ij}}\cdot\left[p_{j,t+1}-p_{i,t+1}+p_{j,t}-p_{i,t}\right]+\\ &\frac{\lambda\Delta t}{4d_{ij}A_{ij}}\left(\frac{M_{i,t+1}^2}{\rho_{i,t+1}}+\frac{M_{j,t+1}^2}{\rho_{j,t+1}}+\frac{M_{i,t}^2}{\rho_{i,t}}+\frac{M_{j,t}^2}{\rho_{j,t}}\right)=0\end{aligned} \tag{14}$$

Note that for the 3rd term in (8), the average value of M^2/ρ is used instead of individual averages for M/ρ assuming that the finite cells are small enough.

In addition to the flow equations, boundary conditions are also set at the ends of the pipes. First, the gas loads at those sink nodes are known as $M_{Di,t}$.

$$M_{i,t} = M_{Di,t} \qquad \forall i \in \text{Sink nodes} \tag{15}$$

And at those source nodes, the gas quality is consistent, i.e., the pressure and density are constant values.

$$\begin{cases} \rho_{i,t} = \rho_{Si,0} \\ p_{i,t} = p_{Si,0} \end{cases} \qquad \forall i \in \text{Source nodes}, t \le T_N \tag{16}$$

According to the previous differencing scheme, observation points are set at both the sending and the receiving ends for every pipeline. If the pipes are connected, there should be a uniform gas density at those intersections, i.e., if nodes $i, i+1, i+2, \ldots$ are connected,

$$\rho_{i,t} = \rho_{i+1,t} = \rho_{i+2,t} \cdots \tag{17}$$

And at the intersections, the mass flow rate should be balanced among the incoming and outgoing pipelines.

$$M_i + M_{i+1} + M_{i+2} \cdots = 0 \tag{18}$$

The gas state equation (7)also applies as the boundary condition for every observation point in the gas system.

$$p_i = c^2 \rho_i \qquad \forall i \tag{19}$$

From the previous derivation, the gas flow is not only determined by the injections and consumptions at the current time step, but also influenced by the gas flow in the previous time step. So in a transient state, the gas flows at different time are interdependent.

Formulation of the Dynamic Optimal Energy Flow Problem

In this section, the dynamic optimal energy flow in the integrated natural gas and electrical power systems is formulated. The basic idea is to combine the steady-state load flow in power system and the differencing form of dynamic gas flow as the equality constraints. Together with operational limits for the facilities, nodal voltage phase angle, and gas pressure, the optimization problem is built to minimize the fuel cost while at the same time reliably supply the demands in both systems. The gas network constraints such as (13) to (17) etc. are linear constraints. However, the deviatoric stress tensor term in gas momentum equation is a nonlinear term with 2nd-order ω and 1st-order ρ multiplied together. The average gas velocity $\bar{\omega}$ can be used to approximate the second-order term.

$$\frac{\lambda}{d}\frac{\omega^2}{2}\rho = \frac{\bar{\omega}\lambda}{2d} \cdot \omega\rho = \frac{\bar{\omega}\lambda}{2d} \cdot \frac{M}{A} \tag{20}$$

Then (8) can be derived as

$$\frac{\partial M}{A\partial t} + \frac{\partial p}{\partial x} + \frac{\lambda\bar{\omega}}{2dA} M = 0 \tag{21}$$

The partial derivatives to time ∂t and axial distance ∂x remain in the linearized equation (21) to reflect the dynamic of the gas flow. Its differencing form becomes linear as follows.

$$\begin{aligned} \frac{1}{A_{ij}} \left(M_{j,t+1} + M_{i,t+1} - M_{j,t} - M_{i,t} \right) + \frac{\Delta t}{L_{ij}} \cdot \left[p_{j,t+1} - p_{i,t+1} + p_{j,t} - p_{i,t} \right] \\ + \frac{\lambda \bar{\omega}_{ij} \Delta t}{4 d_{ij} A_{ij}} \left(M_{j,t+1} + M_{i,t+1} + M_{j,t} + M_{i,t} \right) = 0 \end{aligned} \tag{22}$$

The linepack storage provides major flexibility to the natural gas system. Since the gas system does not have so many kinds of facilities as the power system for regulation purposes, the linepack storage needs to be carefully used and restored after usage. Usually, the gas transmission system is divided into several zones. The restoration time varies with different nations and system operators. In this work, it is required that the linepack storage should be recovered every 24 hours, i.e.

$$\left|\sum_{i\in zone} p_{i,t} - \sum_{i\in zone} p_{i,0}\right| \le \xi \quad \forall\, t = 24I \tag{23}$$

where t is an integer I multiple of 24 hours. And ξ is a small range for the system pressure level to vary. Here let $\xi = 1\% \times \sum_{i\in Zone} p_{i,0}$.

Besides the gas flow, the DC power flow is used in this project to formulate the network constraints. The power flow through the transmission line km can be obtained from the nodal phase angles.

$$f_{km,t} = b_{km,t}(\theta_{k,t} - \theta_{m,t}) \tag{24}$$

It is subject to the thermal limits of the transmission capacity.

$$\left|f_{km,t}\right| \le \overline{f}_{km,t} \tag{25}$$

For each generator $n = 1,2,\ldots$, the real power production should be within its operation limits.

$$\underline{P}_{n,t} \le P_{n,t} \le \overline{P}_{n,t} \tag{26}$$

Ramping limits of the generators excluding the wind farms are also considered as the following.

$$\left|P_{n,t} - P_{n,t-1}\right| \leqslant P_{R,n} \tag{27}$$

And for each period, the real power production and consumption in the electrical system should be balanced.

In this work, bi-directional energy conversion is considered. The GT consumes natural gas to produce electricity. On the contrary, the P2Gs consumes electricity to produce natural gas. For P2Gs, the relationship between the produced gas and consumed power can be represented by:

$$M_{Si,t} = \eta_{ki} P_{Lk,t} \tag{28}$$

The subscription ki indicates that the P2G is converting energy from bus k in the power system to node i in the natural gas system. And the relationship between the electrical power produced by the GTs and the consumed natural gas can be represented by:

$$P_{Gn,t} = \eta_{in} M_{Di,t} \tag{29}$$

The subscription in connects the mass flow rate at Node i and the nth generator. For brevity, the two coefficients η_{ki} and η_{in} here do not only indicate the efficiency of the devices but also embed the unit conversion between mass flow rate and power. So the unit of η_{ki} is kg·MW/s while η_{in} is in MW·s/kg.

The objective function of the optimization problem can be formulated as

$$\min \sum_{t=1}^{T_N} \left(\sum_{n\in\Omega_g} c_{gn} P_{n,t} + \sum_{i\in\Omega_s} c_{si} M_{Si,t} \right) \tag{30}$$

In the objective function, the cost coefficients c_{gn} are set for different generation sites. For the coal-fired generators, a positive c_{gn} minimizes their output to reduce the fossil fuel useage. For the wind farms, c_{gn} =0 so that the renewable energy accommodation is maximized. For the gas-fired generation, its fuel cost is only accounted in the gas system side. The P2G stations are not included in the objective function, but by constraint conditions, P2G stations only convert surplus free electricity to gas (which will be discussed in the case study). So the cost coefficient c_{gn} for the gas-fired generation is also set to 0. In the natural gas system side, a positive cost coefficient c_{si} is set to minimize the gas consumption. The optimization variables include voltage angle, gas pressure and branch flow in two systems, etc. Flows at different time step are linked by the dynamic gas flow and ramping limits of the generators. Though with a considerable scale, the optimization is a linear programming problem and hence can be easily solved.

Case studies

In this work, the combination of IEEE 39-bus power system and the 27-node gas system is built as the test system, as shown in Fig. 18. The branch numbers of the power and gas systems are 29 and 26. In the natural gas system, there are 2 source nodes and 6 sink nodes. Besides, 2 P2Gs and 2 GTs are installed in the system. In the power system, there are 10 generation sites. G3 and G4 are the GTs connected to Node 13 and 22 in the gas network, respectively. G9 and G10 are replaced by two wind farms. The 2 P2Gs are installed at Bus 17 and 22, corresponding to Node 27 and 8 in the gas system, with capacities 100 MW and 80 MW respectively.

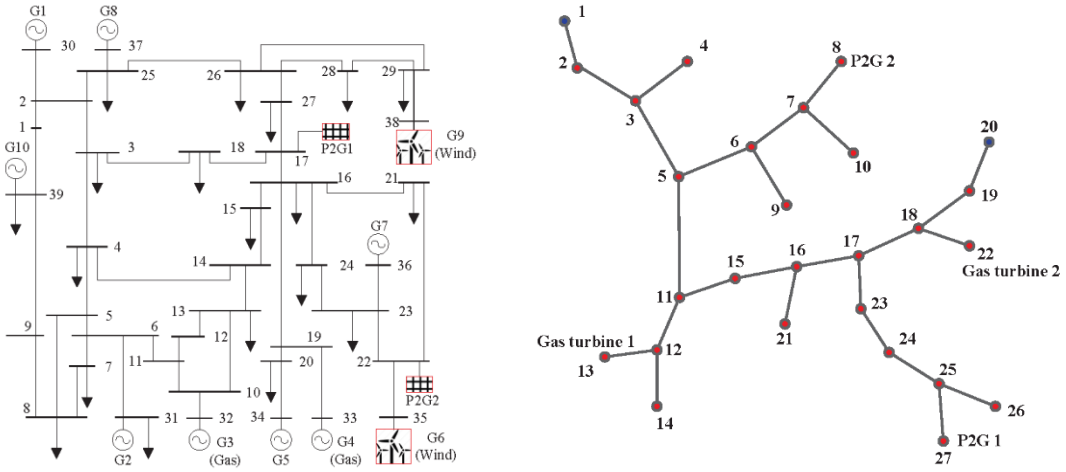

(a) The IEEE 39-bus power system (b) The natural gas system

Fig. 18 The integrated gas and electrical power system.

The annual historical data from Danish power and gas systems is used in this study. The electrical load is between 1308.5 MW and 3607.3 MW, while the gas demand excluding the GT consumption is between 348.5 MW and 4685 MW. The wind power, with its maximum output 3698.6 MW, produces a significant portion of electricity along the year.

For the daily operation of the test system in a 24-hour period, the optimization problem includes 3288 variables, 2762 inequality constraints, and 2376 equality constraints. Since it is a linear programming without binary variables, it is solved very fast. The total computational time is less than 1 second using a personal computer with CPLEX-MatLab linear programming solver.

Fig. 19 shows the optimal operation strategy in a typical day under the high wind condition. For each time period, the height of the bar indicates the total electricity demand. And its distribution among different types of generations, i.e., coal-fired units, gas-fired units, and wind, are shown in different colors. From the figure, one can see that most electrical demand is supplied by the wind generation. The peak load hour is 4.47 GW at 12:00 and 4.34 GW at 18:00. However, a significant amount of wind energy is curtailed from 5:00 to 23:00, as shown in Fig. 19(b).

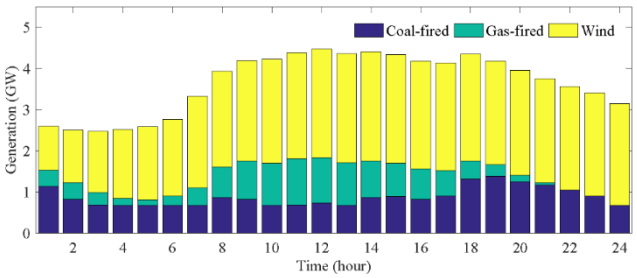

(a) The power generations.

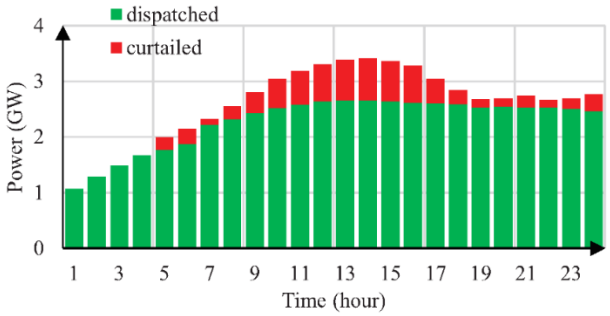

(b) The wind curtailment.

Fig. 19 The operation strategy on the test system.

At the gas system side, Fig. 20 illustrates the gas injections and consumptions. Limited by capacity and efficiency of the P2G, most of the gas comes from the source nodes. In Fig. 20(a), the maximum injections at Node 1 and Node 20 are 42.97 kg/s and 61.62 kg/s at 15:00, respectively. The maximum gas demand and GT consumption are 29.1 kg/s at 8:00 and 21.04 kg/s at 11:00, respectively. Due to the nodal pressure limits, it can be observed that the GTs works when the gas demand is less.

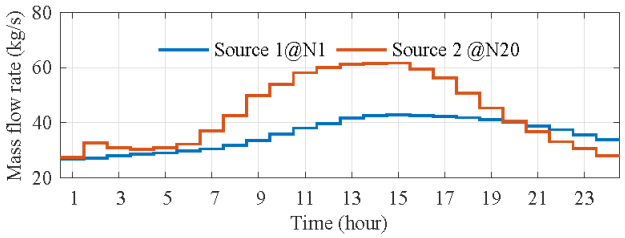

(a) Mass flow rate at the source nodes.

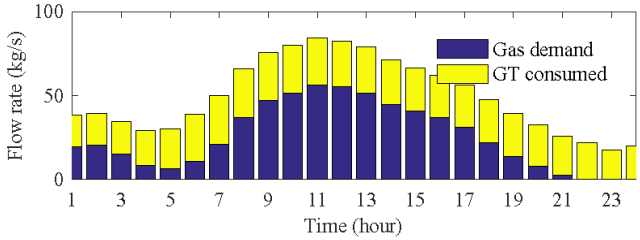

(b) Gas demand in the system and GT consumption.

Fig. 20 Gas source and consumptions under the optimal operating strategy.

The linepack storage of the gas network plays an important role in balancing the production and consumption. Fig. 21 shows average pressure across the gas network. The pressure drops to the minimum 50.96 bar when the linepack storage is consumed before 14:00. After 14:00, the linepack is restored by consuming less and taking more from the source. The average pressure of the system gradually recovers and reaches 51.25 bar at 24:00. Together with Fig. 20, the 'slow' process that the gas network response to the load change can be observed.

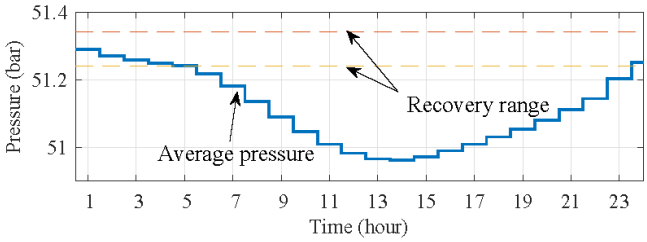

Fig. 21 Average pressure in the gas system.

Further, the detailed transient process in the gas system is presented to demonstrate the advantage of the proposed model. Another day with low wind production is investigated. Fig. 22 illustrates the dynamics of the gas flow in part of the gas networks including node 11 to 14

and associated pipes. The gas demand at Node 14 remains steady during this day. Comparatively, the GT consumption at Node 13 fluctuates more quickly in a broader range and hence has more influence on the pressure of Node 12.

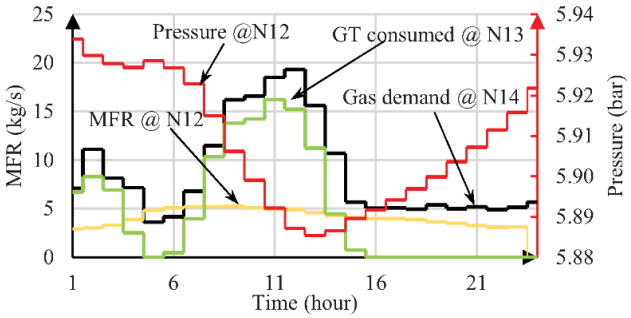

Fig. 22 The nodal pressure varies with the mass flow rate in the gas system

Fig. 23 is the gas dynamics in the pipe from Node 5 to Node 11. Pipe 5-11 is the longest pipe in this gas system. Due to the static effect of the gas dynamics, the difference between the gas pressures at Node 5 and Node 11 increases with the mass flow rate. But different from the steady-state models, it can be seen that the mass flow rate at the sending and receiving ends of this single pipe does not necessarily equal. Fig. 23(a) illustrates the gas density changes with the mass flow rate. For the pipeline connecting Node 5 and Node 11, when the inlet mass flow rate at Node 5 is larger than the outlet flow at Node 11, the pressure and the linepack storage in the pipe increases, and vice versa. With the dynamic flow model for the gas network, it is possible to assess the amount of linepack storage in each single pipes. This leads to a better utilization of flexibility provided by the natural gas grid.

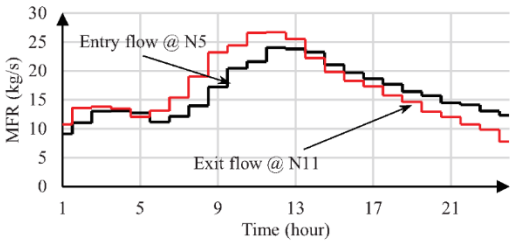

(a) The mass flow rate at two ends of the pipe 5-11.

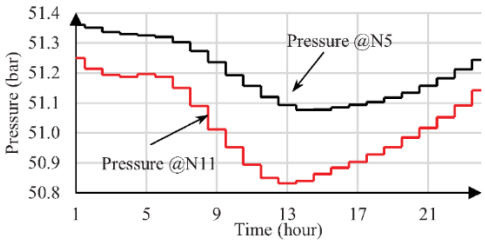

(b) The dynamic change of the gas pressures at Node 5 and 11.

Fig. 23 The dynamic of gas flow through pipe 5-11.

To investigate the influence of incorporating the dynamic gas flow, the optimization results are compared with the static and dynamic gas flow. The terms with partial derivatives to time t in (10) and (11) are removed. The same differencing scheme is used to convert the differential equations to differencing equations as equilibrium constraints in the optimization. With different constraints from the gas system side, different optimization results are obtained, as shown in Fig. 24. Fig. 24(a) illustrates the mass flow rates while Fig. 24(b) shows the gas density variation in Pipe 5-11. Derived from (10), $\partial\rho/\partial t = 0$ leads to $\partial M/(A\partial x) = 0$. Consequently, it can be seen from Fig. 24(a) that without considering the dynamic gas flow, the mass flow rates along the pipe are the same.

With the dynamic gas flow model, the linepack storage can be assessed by

$$Linepack = E_0 + \int_{\tau=1}^{t} M_{in}(\tau) - M_{out}(\tau)\, d\tau \tag{31}$$

where E_0 is the initial amount of gas in the pipe. M_{in} and M_{out} are the inlet and outlet flow rates of the pipe, respectively. Fig. 24(b) shows that the gas stored in the pipe varies with the inlet and outlet flow rates.

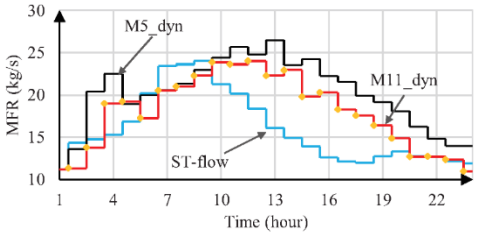

(a) The mass flow rate under the static and transient gas flow.

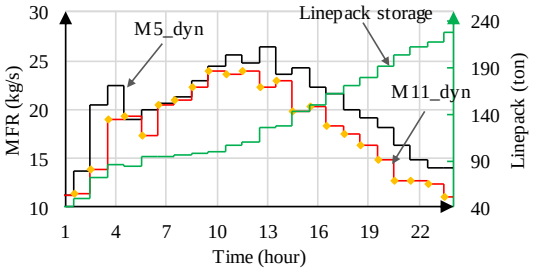

(b) linepack_illustration.

Fig. 24 Comparison between the static and dynamic gas flow in pipeline 5-11. M_5 and M_{11} stands for the mass flow rate at Node 5 and Node 11, respectively.

With the dynamic gas flow considered, the linepack storage in different pipes can be operated in coordination. With other constraints remaining unchanged, the optimization results across the whole year, as shown in Fig. 25. It depicts that incorporating dynamic gas flow improves the system operation from two perspectives. The total gas fuel used to produce electricity is reduced. Besides, more gas production from P2G plants is enabled.

From this comparative study, the necessity of embedding transient gas flow into the integrated power and gas system is demonstrated.

Next, the beneficial role of the P2G is investigated. Fig. 26 shows the annual duration curve of the wind power in the test system. It can be seen that the dispatched wind power increases if the P2G is installed.

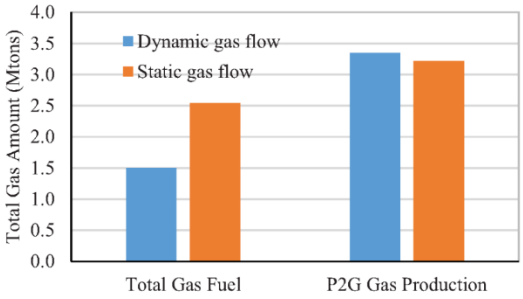

Fig. 25 Annual total gas fuel consumed for electricity production.

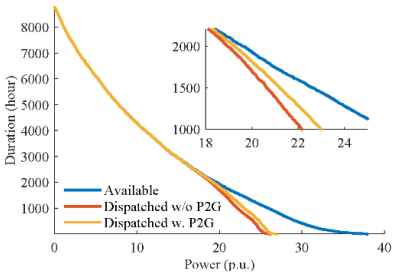

Fig. 26 Wind duration curve with and without P2G.

Connected to the buses far from the wind farms in the power network, the P2G 1 is functioned differently from P2G 2. Fig. 27 (a) shows the unsupplied gas reduction with the P2Gs. Fig. 27 (b) demonstrates that with the larger capacity of P2G 1, the annual unsupplied gas demand reduces. But due to the limited capacity and energy conversion efficiency, very few part of the gas demand is supplied by the P2G production. From the above analysis, the beneficial role of the P2G includes avoiding the network congestions, supplying the gas demand and improving wind power accommodation. The roles of P2Gs at different install locations differ from each other.

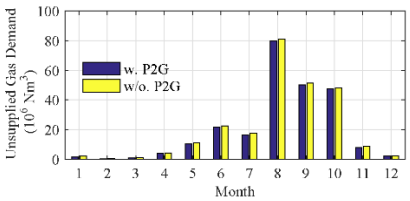

(a) Monthly unsupplied gas demand with and without P2G

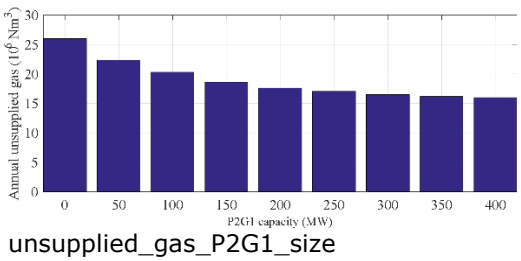

(b) unsupplied_gas_P2G1_size

Fig. 27 The unsupplied gas.

1.5.1.4 Optimal energy flow model for integrated power and heating system

This section investigates the interaction of the heating system with the power system. The study is to investigate an optimal way to integrate the energy of both systems in urban areas. The amount of energy conversion between the electrical system and the heating system was optimally decided so that the demand within both systems could be met at the least operational cost. Besides, the best node to join with the electrical system and heating system was chosen by consideration of the energy transmission loss. **Full content is published Applied Energy entitled 'Optimal operation of the integrated electrical and heating systems to accommodate the intermittent renewable sources.'**

- **Mathematical formulations of the operational constraints in heating system**

The optimization problem for the integrated electrical and heating systems is formulated in this section. The objective function is set as the operational cost. And the nodal energy flow equations are modeled as equality constraints. The operational limits can be categorized as follows. First, the limits to the branches include flow capacities through the pipes and lines, and the maximum temperature drop along with the pipeline. Second, nodal operation limits keep the temperatures and voltages within a reasonable range to maintain the system security. Third, the devices such as heat exchangers, generators, and heat pumps (HPs) should be within their capacities. The objective function and 3 categories of constraints are described in detail in following subsections.

The objective of the optimal operation is to minimize the total operation costs F^{Total} consisting of electrical F^{E} and heating system F^{T} throughout the whole operational horizons (τ_{num}), as shown in (32). (33) and (34) indicate the fuel cost for electricity and heat production, respectively. In both cases, wind power is considered as free so that it will be consumed as much as possible.

$$F^{\mathrm{Total}} = F^{\mathrm{E}} + F^{\mathrm{T}} \tag{32}$$

$$F^{\mathrm{E}} = \sum_{\tau=1}^{\tau_{\mathrm{num}}} \sum_{s=1}^{S_{\mathrm{num}}^{\mathrm{G}}} a_{0,s} + a_{1,s} \times P_{s,\tau}^{\mathrm{G}} + a_{2,s} \times (P_{s,\tau}^{\mathrm{G}})^2 \tag{33}$$

$$F^{\mathrm{T}} = \sum_{\tau=1}^{\tau_{\mathrm{num}}} \sum_{s=1}^{S_{\mathrm{num}}^{\mathrm{Heat}}} \alpha_s \times SP_{s,\tau} \tag{34}$$

The objective function is subjected to the following constraints.

The mass flow balance at node i in the time period τ is formulated as (35). For each node, positive mass flow rate indicates the inflow and negative mass flow rate indicates the outflow. a_{ij} is the element of incidence matrix A. $SQ_{i,\tau}^{CHP}$, $SQ_{i,\tau}^{W}$, $SQ_{i,\tau}^{HS}$, $BQ_{i,\tau}$, and $NQ_{i,\tau}$ are the mass flow rate of CHP, HP, Heat storage (HS), Pipe, and consumers in time period τ, respectively.

$$\begin{aligned} &\sum_{j=1}^{B_{\mathrm{num}}} a_{ij} \times BQ_{i,\tau} + SQ_{i,\tau}^{\mathrm{CHP}} + SQ_{i,\tau}^{\mathrm{HP}} + \\ &(T\_d_{i,\tau}^{\mathrm{dis}} - T\_d_{i,\tau}^{\mathrm{ch}}) \times SQ_{i,\tau}^{\mathrm{HS}} - NQ_{i,\tau} = 0 \end{aligned} \tag{35}$$

The conversion relationships between mass flow rate (t/h) and thermal power (kW) are shown by (36). c is the heat capacity of water, 4.2kJ·kg^{-1}·C^{-1} and 1kWh = 3600J.

$$\begin{aligned} &NQ_{i,\tau} \times (t_{i,\tau} - t_{i,\tau}^{\mathrm{Back}}) \times c - 3.6 \times L_{i,\tau} = 0 \\ &SQ_{i,\tau} \times (t_{i,\tau} - t_{i,\tau}^{\mathrm{Back}}) \times c - 3.6 \times SP_{i,\tau} = 0 \end{aligned} \tag{36}$$

In the heating system, the energy carrier could be both steam and liquid water. In this project, only the heat water is considered for brevity. Eq. (37) Interprets the temperature drop along with the pipeline. The temperature drop coefficient $e_{j,\tau}$ has the relationship with the mass flow rate of the branch $BQ_{j,\tau}$, the length of the branch l_j, and the heat loss coefficient of the branch

γ_j, as shown in (38). The heat loss coefficient γ_j has the relationship with the temperatures of the water t_j, the ambient environment temperature of water t_0, the resistance of channel R_1 and the resistance of insulation material R_2, as shown in (39).

$$\Delta t_{j,\tau} = e_{j,\tau} \times BQ_{j,\tau} \tag{37}$$

$$1000 \times c^T \times (BQ_{j,\tau})^2 \times e_{j,\tau} - 3.6 \times \gamma_j \times (1+\beta) \times l_j = 0 \tag{38}$$

$$\gamma_j = \frac{t_j - t_0}{R_1 + R_2} \quad j = 1,2,\cdots,B^T_{num} \tag{39}$$

To simplify the problem, approximation has been made that the heat loss coefficient γ_j is approximately regarded as a constant. γ_j is chosen according to the temperatures of water and the ambient environment. For example, if R_1=0.0033 W/m.^{0}c, R_2=2 W/m.^{0}c, $95^\circ\mathrm{C} \le t_j \le 100^\circ\mathrm{C}$, $t_0 \approx 100^\circ\mathrm{C}$, then $0 \le \gamma_j \le 2.5$ W/m, and we choose γ_j=2 W/m.

Eq. (40) represents the operational limitations of the heating system including the nodal temperature, branch flow capacity, CHP, Heat pump, and heat storage.

$$\begin{aligned}
&t_i^{\min} \le t_{i,\tau} \le t_i^{\max} \quad i = 1,2,\cdots,N_{\text{num}} \\
&BQ_j^{\min} \le BQ_{j,\tau} \le BQ_j^{\max} \quad j = 1,2,\cdots,B_{\text{num}} \\
&SP_k^{\text{CHP,min}} \le SP_k^{\text{CHP}} \le SP_k^{\text{CHP,max}} \quad k = 1,2,\cdots,S_{\text{num}}^{\text{CHP}} \\
&SP_k^{\text{W,min}} \le SP_k^{\text{W}} \le SP_k^{\text{W,max}} \quad k = 1,2,\cdots,S_{\text{num}}^{\text{W}} \\
&SP_k^{\text{HS,min}} \le SP_k^{\text{HS}} \le SP_k^{\text{HS,max}} \backslash;\backslash;\backslash; \; k = 1,2,\cdots,S_{\text{num}}^{\text{HS}}
\end{aligned} \tag{40}$$

Eq. (41) represents the operational constraints of heat storage. Indicated by (41), the consumed mass flow rate of the heat storage cannot exceed its capacity.

$$\begin{aligned}
&0 \le SQ_{i,0}^{\text{HS}} + \sum_{\tau'=1}^{\tau} (d_{i,\tau'}^{\text{ch}} - d_{i,\tau'}^{\text{dis}}) \times SQ_{i,\tau'}^{\text{HS}} \le SQ_i^{\text{HS,max}} \\
&d_{i,\tau'}^{\text{dis}} + d_{i,\tau'}^{\text{ch}} \le 1 \;\; (d_{i,\tau'}^{\text{dis}}, d_{i,\tau'}^{\text{ch}} = 0 \text{ or } 1)
\end{aligned} \tag{41}$$

The operational constraints of electrical system

The electrical system constraints include active and reactive power balance, nodal voltage, the capacity of traditional generators and lines, and the curtailment of wind power. The detail of each constraint is described as follow.

Nodal active and reactive power balance are considered in this project, formulated as (42). In each node, the electrical power injection needs to be equal to power demand plus losses. Besides, the voltage of each node is limited by (43).

$$\begin{aligned}
&P_{i',\tau}^{\text{G}} + P_{i',\tau}^{W} + P_{i',\tau}^{\text{CHP}} - P_{i',\tau}^{\text{Load}} - U_{i',\tau} \sum_{j' \in i'} U_{j',\tau} (G_{i'j'} \cos\theta_{i'j',\tau} + B_{i'j'} \sin\theta_{i'j',\tau}) = 0 \\
&Q_{i',\tau}^{\text{G}} - Q_{i',\tau}^{\text{Load}} + U_{i',\tau} \sum_{j' \in i'} U_{j',\tau} (G_{i'j'} \sin\theta_{i'j',\tau} + B_{i'j'} \cos\theta_{i'j',\tau}) = 0
\end{aligned} \tag{42}$$

$$U_{i'}^{\min} \le U_{i',\tau} \le U_{i'}^{\max} \quad i' = 1,2,\cdots,N_{\text{num}}^{\text{E}} \tag{43}$$

In the electrical system, active power and reactive power of each source are restricted by the lower and upper bounds, including thermal generators, CHP, and Wind Farm. Also, the limitations of the climbing up/down power during each time interval are considered, as shown in (44).

$$
\begin{aligned}
&P_{i'}^{\mathrm{G,min}} \le P_{i',\tau}^{\mathrm{G}} \le P_{i'}^{\mathrm{G,max}}, \quad i' = 1,2,\cdots,S_{\mathrm{num}}^{\mathrm{G}} \\
&|P_{i',\tau}^{\mathrm{G}} - P_{i',\tau-1}^{\mathrm{G}}| \le P_{i'}^{\mathrm{G,climbe}}, \quad i' = 1,2,\cdots,S_{\mathrm{num}}^{\mathrm{G}} \\
&P_{i'}^{\mathrm{CHP,min}} \le P_{i',\tau}^{\mathrm{CHP}} \le P_{i'}^{\mathrm{CHP,max}}, \quad i' = 1,2,\cdots,S_{\mathrm{num}}^{\mathrm{CHP}} \\
&|P_{i',\tau}^{\mathrm{CHP}} - P_{i',\tau-1}^{\mathrm{CHP}}| \le P_{i'}^{\mathrm{CHP,climbe}}, \quad i' = 1,2,\cdots,S_{\mathrm{num}}^{\mathrm{CHP}} \\
&0 \le P_{i',\tau}^{\mathrm{W}} \le P_{i',\tau}^{\mathrm{W,av}}, i' = 1,2,\cdots,S_{\mathrm{num}}^{\mathrm{W}} \\
&Q_{i'}^{\mathrm{G,min}} \le Q_{i',\tau}^{\mathrm{G}} \le Q_{i'}^{\mathrm{G,max}}, \quad i' = 1,2,\cdots,S_{\mathrm{num}}^{\mathrm{Q}}
\end{aligned}
\tag{44}
$$

Here, we define the curtailment of wind power $P_{i',\tau}^{\mathrm{W,cur}}$ equals to be the available wind power $P_{i'}^{\mathrm{W,av}}$ minus the wind power accommodated $P_{i',\tau}^{\mathrm{W}}$, as shown in(45).

$$
P_{i',\tau}^{\mathrm{W,cur}} = P_{i'}^{\mathrm{W,av}} - P_{i',\tau}^{\mathrm{W}}, 0 \le P_{i',\tau}^{\mathrm{W,cur}} \le P_{i'}^{\mathrm{W,av}}, i' = 1,2,\cdots,S_{\mathrm{num}}^{\mathrm{W}} \tag{45}
$$

Besides, the line transmission limits are considered, formulated by (46). The transfer power from i' to j' should not exceed the line transfer capacities for security consideration.

$$
\left|(U_{i',\tau})^2 G_{i'j'} + U_{i',\tau} U_{j',\tau} (G_{i'j'} \cos\theta_{i'j',\tau} + B_{i'j'} \sin\theta_{i'j',\tau})\right| \le P_{i'j'}^{\max} \tag{46}
$$

The constraints to the interfaces between electrical and heating system

To save the excess wind power at the valley load period, the wind power is partly converted into heat. The obtained thermal energy can be stored in HS or directly injected into the heating system. Due to the limited capacities of HP and HS, maybe not all the surplus wind power can be utilized, and the reduced wind curtailment $\tilde{P}_{i',\tau}^{\mathrm{W,Cur}}$ can be

$$
\eta_{\text{W-T}} \times (P_{i',\tau}^{\mathrm{W,Cur}} - \tilde{P}_{i',\tau}^{\mathrm{W,Cur}}) = d_{i'}^{\mathrm{ch}} \times SP_{i',\tau}^{\mathrm{HS}} + SP_{i',\tau}^{\mathrm{HP}} \quad i' = 1,2,\cdots,S_{\mathrm{num}}^{\mathrm{W}} \tag{47}
$$

The cogeneration unit can output electricity and heat, whose conversion relationship between the electric power and heat is formulated as

$$
SP_{i',\tau}^{\mathrm{CHP}} = P_{i',\tau}^{\mathrm{CHP}} \times (1 - \eta_{i',\tau}^{e} - \eta_{i'}^{I}) / \eta_{i',\tau'}^{e} \times K^{e} \tag{48}
$$

Numerical simulations

A test case is studied here. The heating system consists of two heat sources, 30 pipes, and 31 nodes. CHP and WF are the heat sources. The surplus wind power can be converted to heat that is directly injected into the heating network or stored in heat storage. To reduce the heat loss, it is better to use the heat as soon as possible. Fig. 29 shows the optimal hourly output of electrical and heating power sources throughout the 24 time periods at the lowest operational cost.

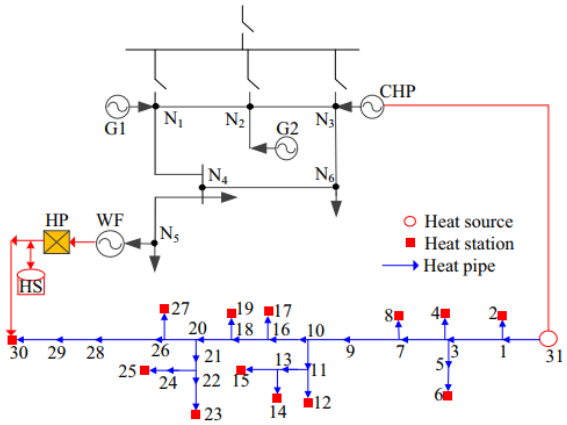

Fig. 28 Studied case of the integrated electrical and heating systems.

In Fig. 29(a), the peak load periods of the electrical system are the valley load periods of the heating system. As Fig. 29(b) showing, during the peak load periods (9th ~ 23rd) of the power system, all the available wind power is consumed in the electrical power system. Hence, in Fig. 29(c), during the 9th ~ 23rd time periods, there is no heat produced by wind power. However, during the periods 1st ~ 8th, the load of the power system is low and the excess wind power is converted into heat, which reduces the wind power curtailment. Also, it can be seen from Fig. 29(b) that the generation of G1 and G2 is smooth and steady. The heating system buffers the production and demand variation and helps to improve the operational efficiency of the thermal units. Fig. 29(d) is the operational process of the heat storage. The HS charges at 3, 5, 7 time periods to reduce the wind curtailment and discharges at 4, 6, 8 time periods to supply the heat load.

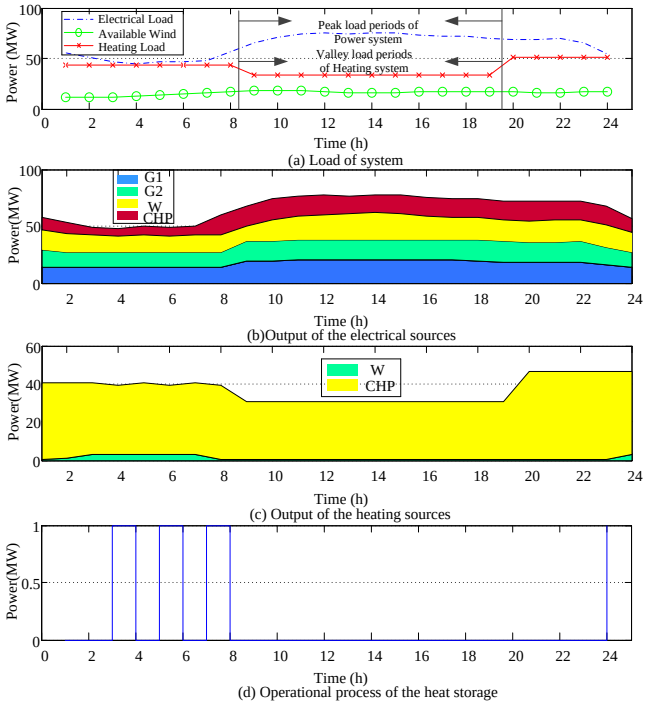

Fig. 29 Optimal dispatch of sources in electrical and heating systems

To show the influence of wind power, Fig. 30 compares the energy distribution in the heating network with and without heat generated by wind power. The curve of the 6th time period is the result with heat generated by wind power while the curve of 16th time period is the result without heat generated by wind power. Reference temperature is assumed to be 100 ℃, though some residential heating systems may have a lower temperature, for example, 60℃. Seen from Fig. 30 (a), without the heat generated by wind power, the temperature is decreasing from Node 1 to Node 30 in the 16th time period. The temperature of Node 26 is higher than Node 25, because they are not along the same transmissions direction. And the temperature from Node 26 to Node 30 is gradually decreasing. While in the 6th time period, it can be seen that the temperatures of Node 27, Node 28, Node 29, and Node 30 are higher than Node 26 because the heat produced by wind power is injected into Node 30. Fig.6 (b) is the corresponding mass flow rate of the branches.

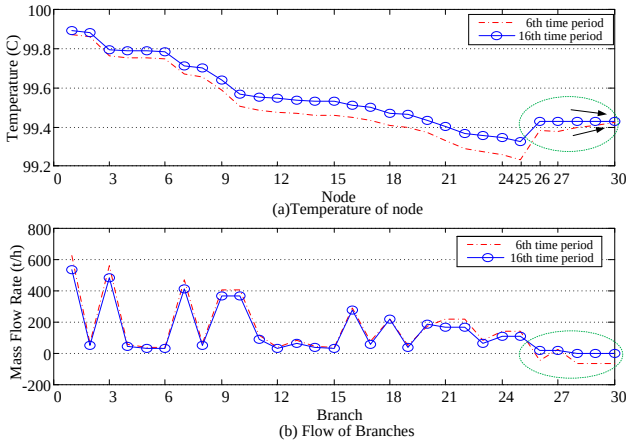

Fig. 30 Temperature drop along the pipes.
(Reference temperature is assumed to be 100 ℃)

Fig. 31 shows the time variation of the nodal temperature and branch flow in the heating system throughout the 24 time periods. The reference temperature is assumed to be 100 ℃ in this case. The nodes and branches illustrated in this figure are located at the sending ends, receiving ends and middle of the whole heating system. In Fig. 31(a), we can see that during the periods 3rd ~ 7th, with the thermal energy produced by the wind power and injected to Node 30, the temperature drop between Node 16 and 30 are less than other time periods. Correspondingly, in Fig. 31(b), the mass flow rate of the Branch 30 is negative and heat load at Node 27 is partly supplied by the HP.

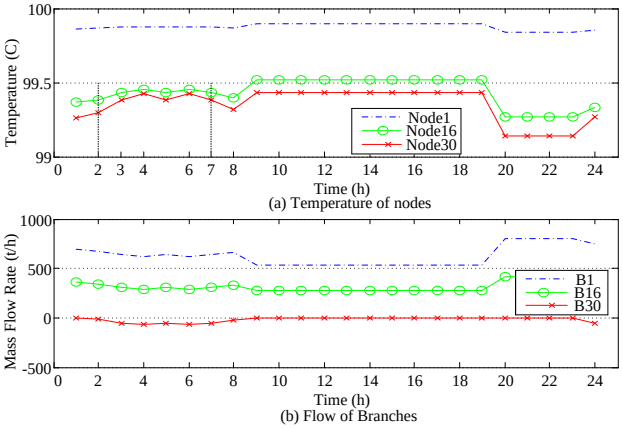

Fig. 31 Nodal temperature and branch's flow in heating system

Comparative studies also have been conducted between individual operation (I-operation) and coordinated operation (Co-operation). Simulation results are shown and analyzed in this section, including curtailment of wind power, the minimum requirement of heat source, and heat loss of the network.

Fig. 32 compares the results of wind power curtailment. During the time periods of 9th~23th, both operation ways have no wind curtailment. Because loads of electrical power system are high during these periods, and all the wind power has been used to balance the electrical power load. In the 2nd ~ 8th time periods, the wind curtailment of Co-operation is much less than that of I-operation.

However, there is still wind curtailment of Co-operation, because the heat pump cannot convert all the wind power to heat due to its power limitation. If the capacity of heat pump is large enough, the wind curtailment can be 0 in the Co-operation mode.

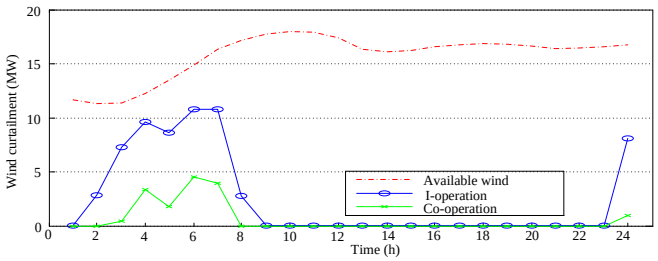

Fig. 32 Comparisons of the wind curtailment with Co-operation and I-operation

Fig. 33 compares the minimum requirements of the heat source. In Fig.11, the requirements of the source of Co-operation are less than the I-operation. The sum of the requirements of heat sources throughout 24 hours is 873 MWh in the mode of Co-operation, while 987 MWh in the mode of I-operation, which is 11.55% higher than Co-operation because more wind power is used to produce heat.

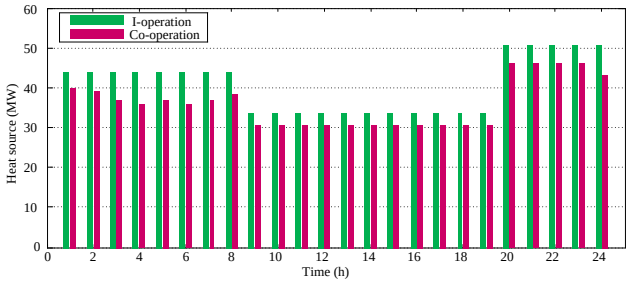

Fig. 33 Comparisons of the requirement of source with Co-operation and I-operation

Fig. 34 compares the heat loss of the heat network. In Fig.12, the heat loss of Co-operation mode is less than which of I-operation. The sum of heat loss throughout 24 hours is 9.54 MW in the mode of Co-operation, while 13.03MW in the mode of I-operation, which is 26.8% higher than Co- operation.

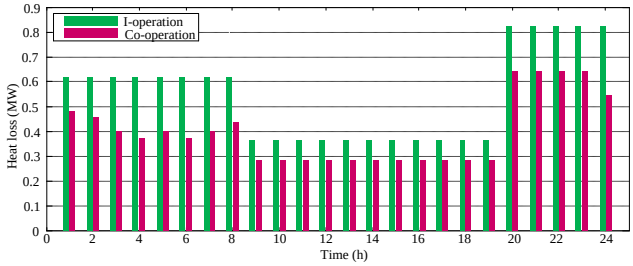

Fig. 34 Comparisons of the heat loss with Co-operation and I-operation

Aggregated modeling and simulation of the Danish district heating and cooling systems

In addition to the detailed heating systems models, the Danish district heating and cooling sector have been comprehensively investigated. **The interim report entitled 'Simulating the Danish DH&C Sector' is attached in the annex**. In the report, aggregated modeling and simulation of Danish district heating and cooling systems are proposed. The approach simulates representative district heating systems for small, medium and large towns. The Danish district heating (DH) sector comprises over 400 individual systems. Applying this approach, we hope to get a clear view on how each type of city should respond to changes in framework conditions. We can subsequently take the results and also scale them to a national level.

To perform the simulations and make the representative setups of district heating systems, data from previous projects: Heating Plan Denmark and Cooling Plan Denmark, are applied. The planning of district heating systems is a complex task involving several entities. Thus, investment and operational costs are project specific. To simplify we use the same specific

costs per plant type. Further, the projected energy prices are used to simulate each system in 2017, 2030 and 2040 with the electricity price from 2016. By annualizing all production costs we can compare a multiple of scenarios for each type of DH system in a simple and foreseeable structure, knowing that in reality the costs will differ.

In this report, how the district heating system will be developed in each setup has been investigated, with special focus on biomass CHP and boilers, heat pumps, electric boilers and combined heating and cooling with aquifer thermal energy storage.

1.5.1.5 Coordinated operation strategy for energy system harmonization

Based on the models built and constraints formulated in the previous sections, the joint operation of the integrated gas, heating and power systems is studied with the aims of maximizing efficiency and minimizing cost. Since weather-dependent renewable sources are considered (e.g., wind power), the model is improved as a two-stage stochastic programming problem. The first stage represents scheduling decisions before the real-time operation for different wind power scenarios, while the second stage represents real-time operating actions. The considered two-stage stochastic formulation allows the optimal scheduling of reserves to facilitate real-time adjustment decisions, which results in minimum cost while integrating the highest level of renewable energy. Several conference papers have been accepted or published and the journal papers are under preparation.

Coordinated operation of electricity, gas and district heating systems

The objective is to minimizes the total system operation cost as shown in Equation (49), which consists of several terms: the operation cost of CHP units to produce electricity and heat, the operation cost of coal-fired power (CFP) units and wind farms (WF) to produce electricity, the cost of gas supply from gas wells (GW), the operation cost of P2G units to produce gas and heat, the operational cost of gas output and gas input of the gas storage, the operational cost of heat output and heat input in the heat storage. The optimization is subjected to electric power constraints, natural gas constraints, district heating constraints and energy conversion limits.

$$\min_{\Xi} \sum_{t=1}^{n^{\mathrm{T}}} \left\{ \sum_{j=1}^{n^{\mathrm{CHP}}} \left(c_j^{\mathrm{CHP,P}} P_{j,t}^{\mathrm{CHP}} + c_j^{\mathrm{CHP,H}} H_{j,t}^{\mathrm{CHP}} \right) + \sum_{i=1}^{n^{\mathrm{CFP}}} c_i^{\mathrm{CFP}} P_{i,t}^{\mathrm{CFP}} + \sum_{f=1}^{n^{\mathrm{WF}}} c_f^{\mathrm{WF}} W_{f,t}^{\mathrm{S}} + \sum_{w=1}^{n^{\mathrm{GW}}} c_w^{\mathrm{GW}} Q_{w,t}^{\mathrm{GW}} \right.$$
$$\left. + \sum_{k=1}^{n^{\mathrm{P2G}}} \left(c_k^{\mathrm{P2G,Q}} Q_{k,t}^{\mathrm{P2G}} + c_k^{\mathrm{P2G,H}} H_{k,t}^{\mathrm{P2G}} \right) + \sum_{s=1}^{n^{\mathrm{GS}}} \left(c_s^{\mathrm{GS,in}} Q_{s,t}^{\mathrm{GS,in}} + c_s^{\mathrm{GS,out}} Q_{s,t}^{\mathrm{GS,out}} \right) + \sum_{h=1}^{n^{\mathrm{HS}}} \left(c_h^{\mathrm{HS,in}} H_{h,t}^{\mathrm{HS,in}} + c_h^{\mathrm{HS,out}} H_{h,t}^{\mathrm{HS,out}} \right) \right\} \tag{49}$$

The illustrative case is given first. Fig. 35 shows a test system considered in this work. This test system includes a 4-bus electricity system, a 3-node heating system and a 4-node gas network. The electricity system is composed of a CHP unit, a CFP unit, and a wind farm. The gas network includes a gas source, a gas storage and a gas compressor. The heating system includes heat storage and three nodes. There are two links: CHP and P2G units.

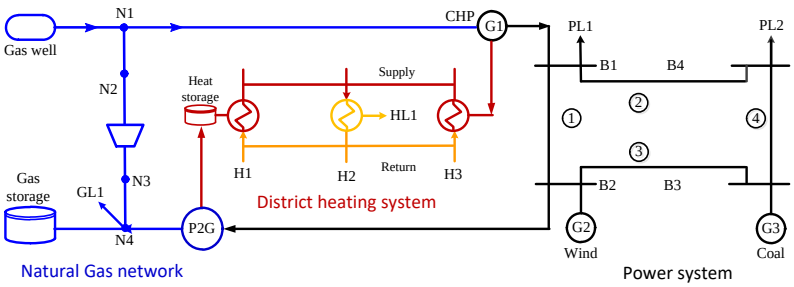

Fig. 35 The structure of an integrated electricity, natural gas and district heating system.

Just as the voltage, which plays a major role in the electrical power system, the gas pressure and water temperature are critical factors for the security operation of natural gas system and district heating system, respectively. Fig. 36 demonstrates the comparison of the simulation results with P2G and without P2G. Fig. 36(a) shows the water temperature at the inlet and

outlet of node 2, which is a load node. The reference temperature is fixed to 100 ℃. As there are heat losses generated during the process of heat transmission, the water temperatures at the inlet of node 2 are lower than the reference node. Besides, there is a lot of heat exchange happen at the load node. Thus the water temperature at the outlet of node 2 will be further declined. The level of temperature drop at load node mainly depends on the amount of heat load. It shows that the temperature drop is larger during the higher heat demand hours. Finally, due to heat supply from P2G unit, the inlet and outlet temperatures of the integrated system with P2G are higher than that without P2G. A higher outlet temperature helps to guarantee normal operation of heating network. Fig. 36(b) shows the variability of nodal gas pressure. The reference pressure is fixed to 1 bar. It shows that the variability of nodal gas pressure can be smoothed by installing P2G in the multi-energy systems. Further, the nodal gas pressure varies in a narrow range, which indicates that the gas system can play a stabilizing role in multi-energy systems as there is gas linepack in the operational process. It is illustrated that both the district heating system and the natural gas system can provide flexibility to accommodate the fluctuation of the electrical power system.

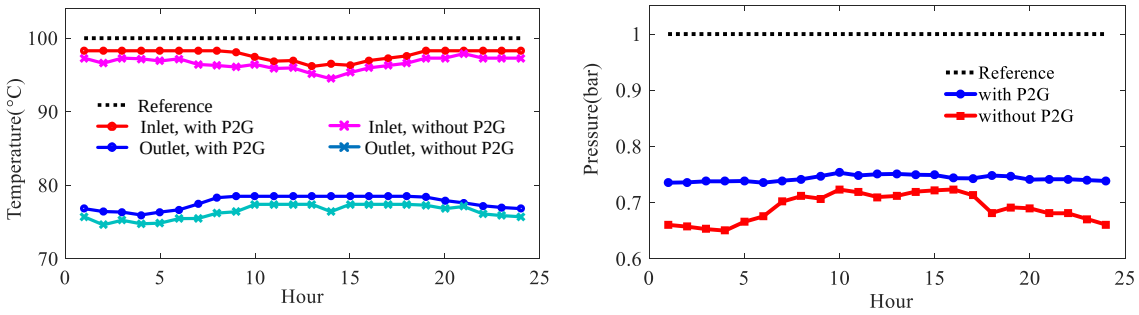

Fig. 36 Network operational parameters: (a) node 2 at the district heating system, (b) node 4 at the natural gas system.

This subsection analyzes the scheduling strategy throughout a 24-hour time horizon. Fig. 37(a) illustrates the optimal schedule of the electrical system. The total electricity consumption is composed of the power system load and the electricity consumption at the P2G unit. In this case, there is a high wind power output, but only a small amount of surplus wind power is curtailed in the night. Most of the excess electricity is converted into gas and heat by the P2G unit, which helps to reduce the wind curtailment. Fig. 37(b) illustrates the optimal schedule of the gas system. The total gas consumption includes both the gas demand and the gas consumption at CHP unit. The difference between gas production and consumption is balanced by linepack storage which shown as the difference between the total gas consumption and the colored area. It shows that the linepack storage provides the flexibility to gas networks. Fig. 37(c) illustrates the optimal schedule of district heating system. The total heat consumption includes the heat load and the heat loss. The heat loss comes from the heat dissipation of the high-temperature water. There is about 12.4% of heat loss in this study. The difference between heat supply and heat consumption is balanced by the heat storage which shown as the difference between the total heat consumption and the colored area.

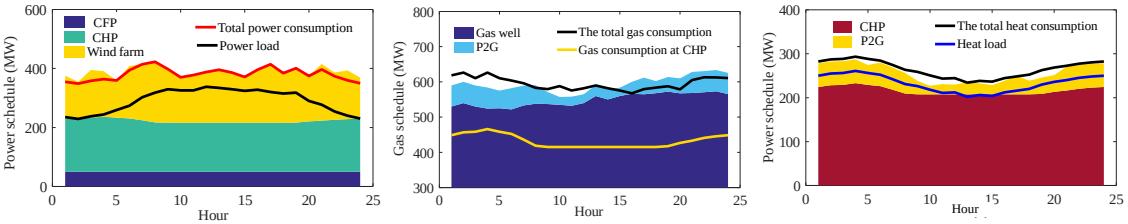

Fig. 37 Optimal schedule of sources: (a) the electrical system, (b) the natural gas system, (c) the district heating system.

With the increasing deployment of renewable sources, such as wind power in power systems, uncertainties become important. This section provides a model to jointly operate the electricity, gas and district heating systems of a city under uncertainty with the aims of minimizing cost.

The weather-dependent electricity sources are considered (e.g., wind power), the model is formulated as a two-stage stochastic programming problem. The first stage represents scheduling decisions prior to real-time operation for different wind power scenarios, while the second stage represents real-time operating actions. The model is illustrated using the energy system of a city that includes a gas subsystem with a gas well and a gas storage facility, and electricity subsystem that includes a coal-fired power plant, a combined heat and power unit and a power-to-gas facility, and a conventional district heating subsystem.

The objective is to minimize the total expected system operation costs, which include both the cost related to the day-ahead energy scheduling and the expected cost of the anticipated balancing actions to be taken during the real-time operation of the integrated energy system. The objective function is subject to two different sets of constraints, namely, the scheduling constraints and the real-time operation constraints.

$$
\begin{aligned}
&\min_{\Xi} \sum_{t=1}^{n^{\mathrm{T}}} \Bigg\{ \sum_{j=1}^{n^{\mathrm{CHP}}} \left(c_j^{\mathrm{CHP,P}} P_{j,t}^{\mathrm{CHP}} + c_j^{\mathrm{CHP,H}} H_{j,t}^{\mathrm{CHP}} \right) + \sum_{i=1}^{n^{\mathrm{CFP}}} c_i^{\mathrm{CFP}} P_{i,t}^{\mathrm{CFP}} + \sum_{f=1}^{n^{\mathrm{WF}}} c_f^{\mathrm{WF}} W_{f,t}^{\mathrm{S}} + \sum_{w=1}^{n^{\mathrm{GW}}} c_w^{\mathrm{GW}} Q_{w,t}^{\mathrm{GW}} + \\
&\sum_{k=1}^{n^{\mathrm{P2G}}} \left(c_k^{\mathrm{P2G,Q}} Q_{k,t}^{\mathrm{P2G}} + c_k^{\mathrm{P2G,H}} H_{k,t}^{\mathrm{P2G}} \right) + \sum_{s=1}^{n^{\mathrm{GS}}} \left(c_s^{\mathrm{GS,in}} Q_{s,t}^{\mathrm{GS,in}} + c_s^{\mathrm{GS,out}} Q_{s,t}^{\mathrm{GS,out}} \right) + \sum_{h=1}^{n^{\mathrm{HS}}} \left(c_h^{\mathrm{HS,in}} H_{h,t}^{\mathrm{HS,in}} + c_h^{\mathrm{HS,out}} H_{h,t}^{\mathrm{HS,out}} \right) \Bigg\} \\
&+ \sum_{\omega \in \Phi} \pi_\omega \sum_{t=1}^{n^{\mathrm{T}}} \Bigg\{ \sum_{j=1}^{n^{\mathrm{CHP}}} \left[c_j^{\mathrm{CHP,P}} \left(PR_{j,\omega,t}^{\mathrm{CHP,U}} - PR_{j,\omega,t}^{\mathrm{CHP,D}} \right) + c_j^{\mathrm{CHP,H}} \left(H_{j,\omega,t}^{\mathrm{CHP}} - H_{j,t}^{\mathrm{CHP}} \right) \right] + \sum_{i=1}^{n^{\mathrm{CFP}}} c_i^{\mathrm{CFP}} \left(PR_{i,\omega,t}^{\mathrm{CFP,U}} - PR_{i,\omega,t}^{\mathrm{CFP,D}} \right) \\
&+ \sum_{w=1}^{n^{\mathrm{GW}}} c_w^{\mathrm{GW}} \left(Q_{w,\omega,t}^{\mathrm{GW}} - Q_{w,t}^{\mathrm{GW}} \right) + \sum_{k=1}^{n^{\mathrm{P2G}}} \left[c_k^{\mathrm{P2G,Q}} \left(QR_{k,\omega,t}^{\mathrm{P2G,U}} - QR_{k,\omega,t}^{\mathrm{P2G,D}} \right) + c_k^{\mathrm{P2G,H}} \left(H_{k,\omega,t}^{\mathrm{P2G}} - H_{k,t}^{\mathrm{P2G}} \right) \right] \\
&+ \sum_{s=1}^{n^{\mathrm{GS}}} \left[c_s^{\mathrm{GS,in}} \left(Q_{s,\omega,t}^{\mathrm{GS,in}} - Q_{s,t}^{\mathrm{GS,in}} \right) + c_s^{\mathrm{GS,with}} \left(Q_{s,\omega,t}^{\mathrm{GS,out}} - Q_{s,t}^{\mathrm{GS,out}} \right) \right] + \sum_{h=1}^{n^{\mathrm{HS}}} \left[c_h^{\mathrm{HS,in}} \left(H_{h,\omega,t}^{\mathrm{HS,in}} - H_{h,t}^{\mathrm{HS,in}} \right) + c_h^{\mathrm{HS,out}} \left(H_{h,\omega,t}^{\mathrm{HS,out}} - H_{h,t}^{\mathrm{HS,out}} \right) \right] \\
&+ \sum_{f=1}^{n^{\mathrm{WF}}} c_f^{\mathrm{WF}} \left(W_{f,\omega,t} - W_{f,\omega,t}^{\mathrm{spill}} - W_{f,t}^{\mathrm{S}} \right) + \sum_{d=1}^{n^{\mathrm{ED}}} V_d^{\mathrm{LOL}} D_{d,\omega,t}^{\mathrm{ED,shed}} \Bigg\}
\end{aligned}
\tag{50}
$$

This objective function consists of several terms as shown in Equation(50). The first term represents the operation cost of scheduling CHP units to produce electricity and heat. For the gas-fired CHP units, the operation cost does not include the fuel cost as it is computed as a part of the total cost of gas supply. The second and third terms represent the operation cost of scheduling coal-fired power (CFP) units and wind farms (WF) to produce electricity, respectively. The fourth term represents the cost of gas supply scheduling from gas wells (GW). The fifth term represents the operation cost of scheduling P2G units to produce gas and heat. The sixth term represents the operational cost of gas output and gas input of the gas storage in the scheduling stage. The seventh term represents the operational cost of heat output and heat input in the heat storage in the scheduling stage. The eighth to fourteenth terms represent the expected balancing cost of operating the CHP, CFP, gas well, P2G, gas storage, heat storage and wind farms of the integrated system in real-time operation. The fifteenth term represents the cost of any load that must be shed in real-time operation.

As mentioned previously, there are two different sets of constraints: the scheduling constraints and the real-time operation constraints. Each set of constraint is further divided into four types of constraints, which are the electricity, gas, district heating, and the energy conversion devices interfacing different energy systems. In addition, we build the general formulation on the following assumptions to simplify the two-stage stochastic programming model:

1) For the electricity system, the DC power flow model is used. Power losses are ignored.

2) For the gas network, it is assumed that all nodal gas pressures are within normal ranges. Nodal gas flow balances, the facility capacities and the pipeline transmission limits are considered in the gas network constraints.

3) For the district heating network, it is assumed that the water temperature and the water pressure are within normal ranges. The nodal heat flow balance, heat supply capacities and heat transmission limits are considered in the heat network constraints.

4) Upward and downward reserves for CFP, CHP and P2G units are scheduled to compensate high/low wind power production.

5) For simplicity, the gas flow rates and heat flow rates are converted to power units, and the per-unit system used.

The optimal scheduling strategy of the integrated energy system is analyzed throughout a 24-hour time horizon. Fig. 38(a) shows the optimal schedule of the power units. It should be mentioned that the total power consumption includes both the power demand and the electricity consumed by the P2G unit. Conversely, the gas-fired CHP unit plays a critical role regarding peak regulation. On the gas system side, Fig. 38(b) illustrates the gas injections and consumptions. Since there is wind power surplus in the scheduling stage, the excess electricity is converted into gas and heat by the P2G unit, which reduces wind power curtailment. Note that the gas supply from the gas well is flat. The difference between gas supply and consumption is balanced by the gas storage and linepack. In the gas system, there are not as many regulation facilities as in the power system. So, the linepack plays an important role in balancing gas production and consumption. At the district heating system side, Fig. 38(c) illustrates the heat supplies and consumptions. The difference between heat supply and heat consumption is balanced by the heat storage.

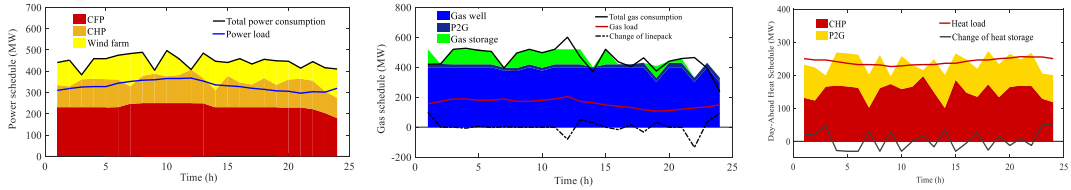

Fig. 38 Optimal schedule of sources: (a) the electrical system, (b) the natural gas system, (c) the district heating system.

The developed model that is reported in this project allows jointly operating the electricity, gas and district heating systems of a city to achieve an efficient and economical performance. This joint operation scheme for all subsystems (electricity, gas and district heating) is clearly better than the independent operation of each of these subsystems. The considered two-stage stochastic formulation allows the optimal scheduling of reserves to facilitate real-time adjustment decisions, which results in minimum cost while integrating the highest level of wind energy. The required computational time is small and clearly compatible with operation requirements

The impact of the uncertainty on the total system operation cost

We can use stochastic programming model to assess the impact of the uncertain wind power production on the expected value of the total system operation cost. Table 3 includes a breakdown of this cost into energy production and reserve capacity costs. For ease of comparison, Table 3 provides an illustration of this cost breakdown, which is calculated for four different cases, namely:

Case a) No uncertainty: the future wind power production is perfectly known, and it coincides with its expected value.

Case b) No wind production: the wind farm is removed from the system. Therefore, loads are exclusively supplied by the thermal units.

Case c) Uncertain wind production: wind power production is uncertain. Results in this case are directly obtained by solving optimization problem.

Case d) Network congestion: wind power production is uncertain as in case (c), and the capacity of one single transmission line in the system is reduced from 200 to 40 MW.

Table 3 Comparison of the expected cost breakdown

Case	a	b	c	d
Energy cost	398650	455735	401740	424864
Reserve cost	0	0	31206	25812
Total cost	**398650**	**455735**	**432946**	**450676**

By comparing case (a) or (c) with case (b), it becomes clear that wind generation leads to a significant reduction in the costs of energy production. The expected cost in case (a) is significantly smaller than in case (c). This difference is largely driven by the cost of the reserve capacity required to cope with wind production uncertainty. Case (d) highlights the key role played by the line capacity. If the capacity of the single line in the system is not high enough, a part of the wind power production is likely to be wasted and the power system will not fully benefit from the cost-free generation of the wind farm. Under faulty conditions, such as outrage of a line or a component, the system cost will be further increased.

1.5.1.6 Multi-stage planning of integrated gas and power systems

This section focuses on the coordinated expansion planning of the integrated natural gas and electrical power systems with bi-directional energy conversion. Both the Gas-fired Power Generation (GPG) and Power-to-Gas plant (P2G) are considered as the linkages between the natural gas and electric power systems. The system operation is optimized and embedded in the planning horizon. A bi-level multi-stage programming problem is formulated to minimize the investment cost plus the operational cost as shown in Fig. 39. The upper-level optimizes the expansion plan determines the network topology as well as the generation capacities, while the lower-level is formulated as an optimal economic dispatch under the operational constraints given by the upper-level decision. To solve the bi-level multi-stage programming problem, a hybrid algorithm is proposed combining the modified binary particle swarm optimization (BPSO) and the interior point method (IPM). The BPSO is used for the upper-level sub-problem, and the IPM is adopted for the lower-level sub-problem.

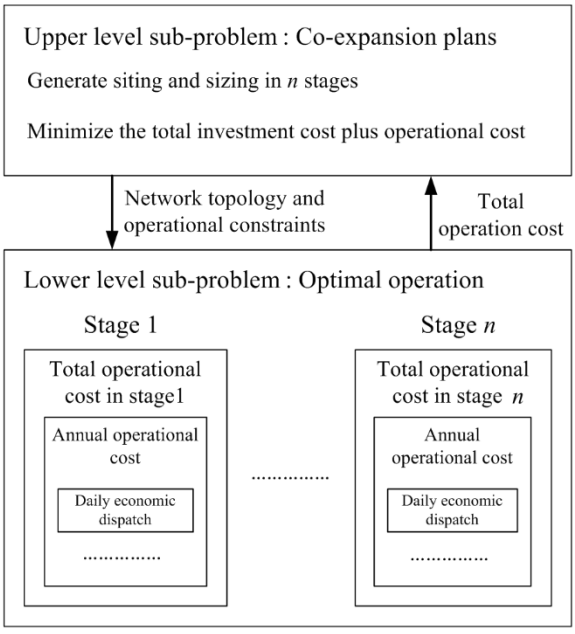

Fig. 39 Framework of bi-level programming on co-expansion planning

Fig. 40 shows the detailed flowchart of solving bi-level programming with the hybrid algorithm. The steps of the hybrid algorithm applied on the bi-level programming are as follows:

1. A group of particles are initialized randomly by a heuristic rule, regarding random position and speed. All the particles provide the network topology and operational limitations.

2. Based on the provided network topology and operational limitations on the upper level, the operational cost can be calculated on the lower level by using IPM.

3. The investment cost can be easily calculated as it is the function of the decision variables of planning given by the position of the particles. Thus, the fitness function of the upper level can be calculated which is the sum of the total investment cost and the operational cost.

4. After the fitness evaluation, the local optimum solution and the global optimum position can be updated. Calculate the particle's velocity in next step, and update the positions of the particles. The speed and position of the particles are determined from the probability point of view.

5. If the lowest investment cost plus operational cost has not changed very much for several times or the iterations meet the maximum number, ends the PSO calculation. Otherwise, back to step 2.

It should be mentioned that the symbol Y represents year, the symbol D represents day. Numerical case studies have been carried out on the practical gas and electricity transmission network in western Denmark. Simulation results demonstrate the effectiveness of the proposed approach.

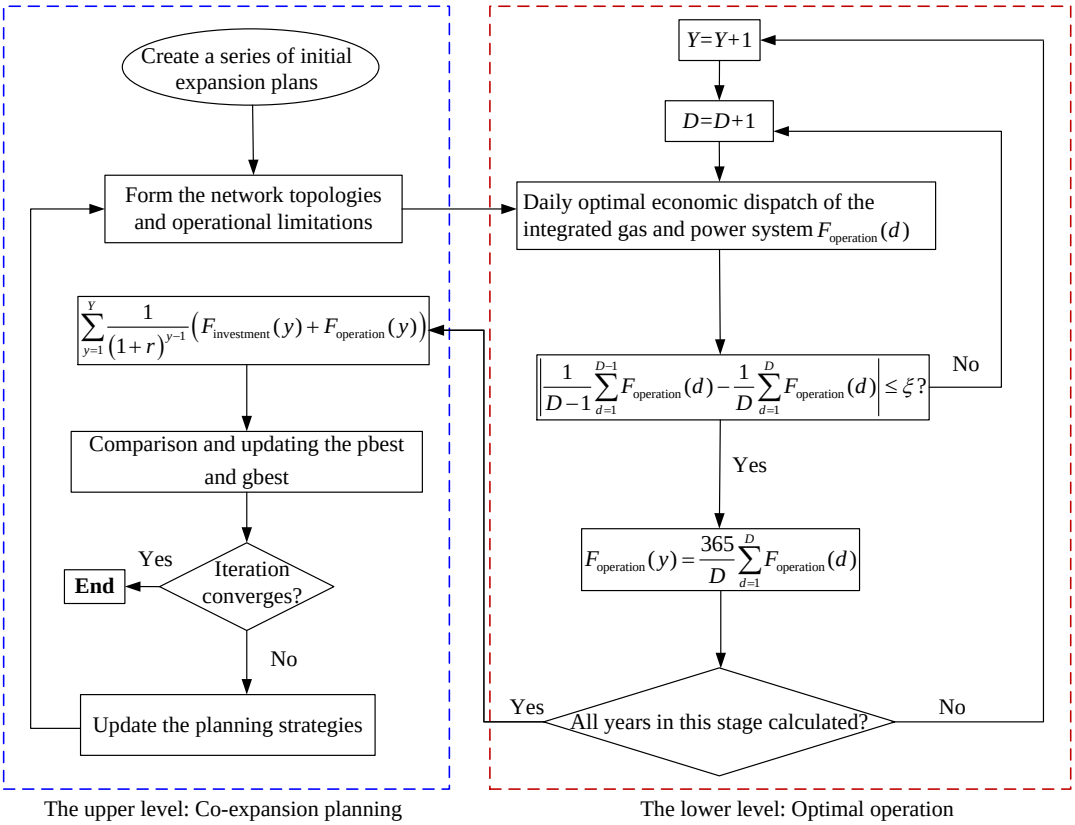

Fig. 40 Flowchart of solving bi-level programming with the hybrid algorithm

The proposed bi-level programming for multi-stage co-expansion planning is illustrated by using the gas and electricity transmission network in western Denmark, as depicted in Fig. 41. The system parameters are obtained from the report published by Energinet.dk, the transmission system operator for electricity and natural gas in Denmark.

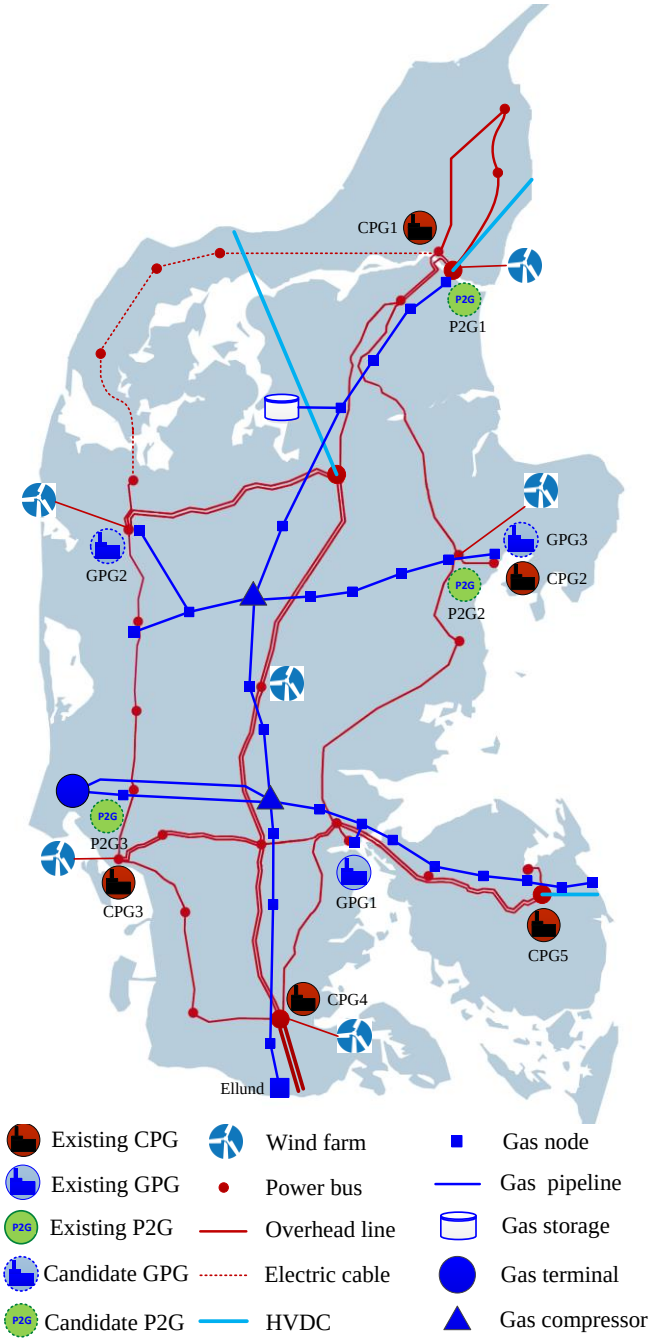

Fig. 41 The natural gas and electricity transmission system in western Denmark.

Scenario Forecast and the Investment Costs

The planning horizon is set nine years (2016–2024) in this project and divided into 3 stages with 3 years in each stage. The detailed forecast shown in Table 4 is also obtained from Energinet.dk.

Table 4 The Energinet.dk's forecast of the planning horizon (2016–2024)

Year	Coal price	Gas price	CO_2 price	Electricity prices	Electricity load	Wind capacity	Percentage of wind
	€/MWh	€/MWh	€/ton	€/MWh	GWh	MW	%
2016	8.1	21.3	7.3	30	20737	5041	41
2017	8.8	22.9	8.8	29.1	20959	5191	43
2018	9.6	24.8	10.8	36.3	21208	5341	45
2019	10.5	26.9	13.5	43.6	21384	5541	48
2020	11.5	28.9	16.8	50.9	21552	6341	58
2021	11.6	29.4	18.1	51.3	21841	6591	61
2022	11.7	29.7	19.5	53.2	22205	6841	64
2023	11.7	30.1	20.7	53.7	22512	6891	66
2024	11.8	30.4	22	54.3	22866	6941	66

In this table, the average prices for the fuels, electricity and CO_2 emission are illustrated as well as the future capacity expansion of electricity consumption and wind power in Denmark. From the consumers' side, Danish electricity consumption is growing slowly. The annual average increase is approximately 1% from 2016 to 2024. From the generation side, it has been estimated by Energinet.dk that 6941 MW wind power will be integrated into the Danish power system, producing 66% of total electricity by 2024, with the annual increase approximately 3.5% from 2016.

The investment in the new plant is divided into two parts: the fixed installation cost wherever there exists no such plant before, and the sizing cost proportional to the capacity. The fixed installation cost makes the existing location as a preferred choice which helps to improve the sustainability of the existed location.

This work assumes that it takes 0.27 million Euro and 0.13 million Euro fixed installation cost to set up a new P2G and GPG plant, respectively. Regarding the sizing costs, it is 2 million Euro/MW for P2G, 0.8 million Euro/MW for GPG and 1.5 million Euro/MW for CPG to both the existing and new plants.

Besides, the nominal cost to shut down the existed CPG and GPG is 0.1 million Euro/MW. Further, a pipeline with a diameter of 100 mm (4 inches) is selected for the transportation of CO_2 gas from the central power plants to the P2G systems. Its investment cost is about 0.08 million Euro/km. The lengths of the CO_2 pipelines are 10km, 15km, and 30km for P2G1, P2G2, and P2G3, respectively. The lifespan is assumed to be 40 years for GPG and 30 years for P2G, and 40 years for CO_2 pipelines.

The multistage evolution of the capacities for P2G, GPG, and CPG

To validate the proposed approach, we carry out the case study on the western Danish electricity and natural gas system. Three different scenarios are studied. Scenario 1 assumes that the annual growth rate of the wind power production is 2%. In Scenario 2, 3.5% of annual growth is assumed and 5% for Scenario 3. The system planning horizon is nine years (2016–2024) consisting of 3 stages. The CPU core used for simulations is 3.06 GHz, the iteration times and particle sizes are set to 50 and 250. The iterative processes of the BPSO for the three scenarios are shown in Fig. 42. It takes less than 150 steps to update before convergence and the computation time are 1054, 1205 and 1146 minutes for Scenario 1, 2 and 3 respectively. It can be considered acceptable for the planning studies. Hence, the result indicates that the proposed method is applicable for the multi-stage expansion co-planning in a real application. The optimization results are shown in Table 5. When the wind power production is higher, the operational cost decreases since less fuel such as gas and coal is burned. However, more investment on the GPG and P2G is needed to ensure the secure energy supply.

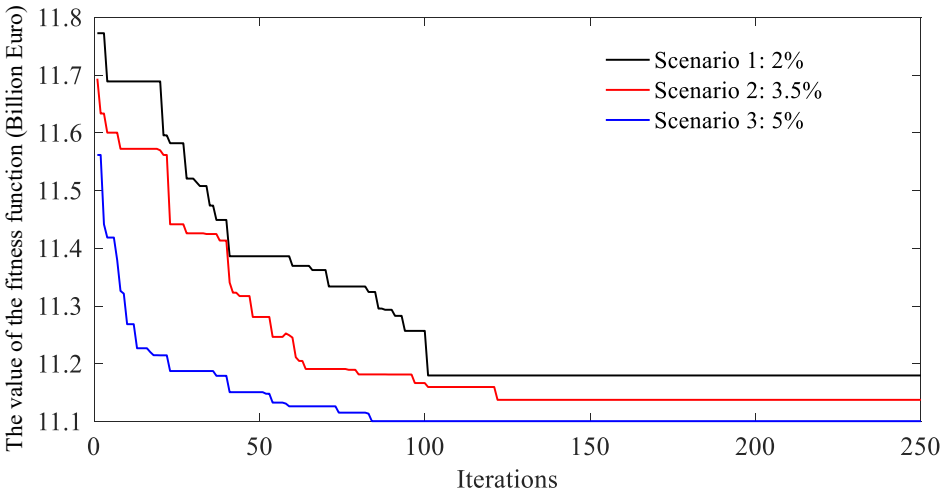

Fig. 42 Optimization process of the proposed method

Table 5 Total expansion and operation cost in billions of Euro

Scenario no.	*Iteration steps before convergence*	*Initial fitness value*	*Optimal total cost*	*Investment cost*	*Operation cost*
Scenario 1	101	11.78	11.18	0.17	11.01
Scenario 2	119	11.69	11.14	0.23	10.91
Scenario 3	82	11.56	11.10	0.24	10.86

The multi-stage evolution of the energy mix is shown in Fig. 43. It can be seen that the capacity of CPG decreases with the increase of the wind penetration level. Meanwhile, the capacities of both GPG and P2G increase at the same time. For scenario 1, the capacity of the CPG is shrunk from 2685MW to 2181MW, while the total capacity of GPG increased from 400MW to 505MW. 208MW P2G plants are planned. For scenario 2, the capacity of the coal-fired power plant is reduced from 2695MW to 2029MW, while 140 MW GPG (increased from 400MW to 540MW) is newly installed. 295 MW P2G is planned in this scenario. Scenario 3 assumes 5% annual growth in the wind power production. The capacity of CPG will be reduced to 1885MW. Additional 166 MW GPG and 351MW P2G are planned in Scenario 3. As can be seen from the comparison of 3 scenarios, the higher the growth rate of wind power can result in more CPG shut down, and faster-growing capacities of GPG and P2G.

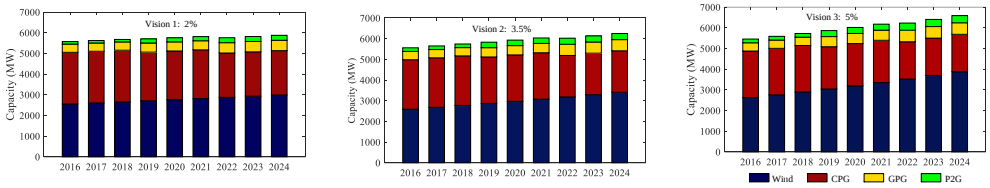

Fig. 43 Evolution of the installed generation from 2016 to 2024 for three scenarios

As shown in Fig. 41, the candidate locations for P2Gs are near the wind farms. So in this case study, P2Gs consumes the surplus wind power in all the three scenarios to reduce the fuel cost for electricity generation. The difference is that the lengths of the CO_2 pipelines are 10km, 15km, and 30km for P2G1, P2G2, and P2G3, respectively. So the investment cost of P2G2 is larger than that of P2G1, and the investment cost of P2G3 is the highest if taking the cost of CO_2 pipelines into consideration. Table 4 illustrates the detailed capacity evolution at each candidate location. P2G1 is the preferred option among the 3 candidate locations. So the capacity of P2G1 grows faster than P2G2. P2G3 is only suggested in scenario 3 with the highest penetration of wind power. For CPGs and GPGs, it can be seen that with the wind power increases, the part of the units at CPG2 is suggested to be shut down and replaced by newly installed gas turbines installed at GPG3. GPG3 has a lower investment cost in comparison with GPG2 because GPG2 requires the fixed installation cost for the initial construction of a newly

selected location. So the existing location GPG3 is a preferred choice to install new gas-fired power generators.

Table 6 Detailed planning strategy in different sites

Candidate location	Initial capacity	Scenario 1			Scenario 2			Scenario 3		
		Stage1	Stage2	Stage3	Stage1	Stage2	Stage3	Stage1	Stage2	Stage3
P2G1	**0**	**91**	**91**	**121**	**100**	**140**	**170**	**78**	**162**	**162**
P2G2	**0**	**59**	**87**	**87**	**75**	**125**	**125**	**90**	**90**	**135**
P2G3	**0**	**0**	**0**	**0**	**0**	**0**	**0**	**54**	**54**	**54**
GPG1	400	400	400	400	400	400	400	400	400	400
GPG2	0	0	0	0	0	0	0	0	0	0
GPG3	**0**	**0**	**48**	**105**	**0**	**56**	**140**	**0**	**90**	**166**
CPG1	410	410	410	410	410	410	410	410	410	410
CPG2	**800**	**684**	**504**	**296**	**530**	**360**	**144**	**460**	**240**	**0**
CPG3	400	400	400	400	400	400	400	400	400	400
CPG4	665	665	665	665	665	665	665	665	665	665
CPG5	410	410	410	410	410	410	410	410	410	410

The optimal daily operation of the integrated gas and electricity system

In this subsection, the optimal operation strategy of the integrated gas and power system is investigated. Fig. 44 shows the optimal operation strategy of the power units in a typical day with high wind. During the peak load periods (7:00 AM~13:00 PM, 17:00 PM~18:00 PM), all the available wind power is utilized to supply the electrical load. Moreover, both the GPG and CPG increase their unit outputs to balance the power demand. During the midnight (12:00 PM~6:00 AM), the excess wind power is converted into gas fuel by P2G. Due to the limitation of the available capacities of the P2G, there is still some wind curtailment in this period but reduced by using P2G. It should be mentioned that the total power load includes both the nodal power demand and electricity consumed by P2G.

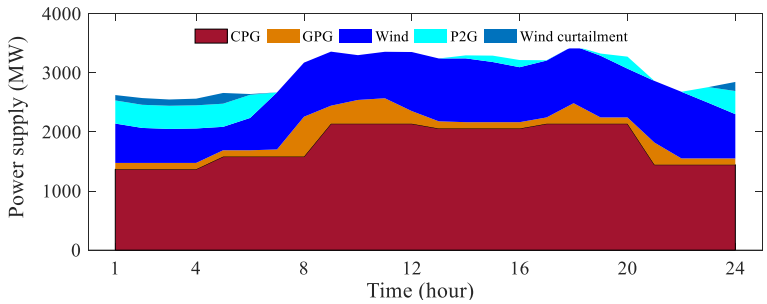

Fig. 44 Daily economic dispatch at power system side.

Note that in Fig. 43, the total wind power output is divided into three parts: part 1 is supplied to meet the power load shown as blue; part 2 is used for gas production in P2G shown in bright blue; the rest is curtailed shown in dark blue.

At the gas system side, Fig. 45 illustrates the gas injections and consumptions. It shows that the gas supply from the gas terminal and gas storage appears to be a constant value. Besides, P2G only converts the surplus wind power due to the efficiency considerations. The difference between the gas supply and consumption is balanced by the linepack. It can be seen that the linepack is consumed in the day and restored in the midnight. In the peak-gas-demand hour (e.g. 8:00AM~13:00 PM), the increasing gas demand from GPG leads to a rapid linepack consumption. In the gas system, there are not as many regulation facilities as the power

system. So the sufficient linepack storage plays an essential role in balancing gas production and consumption.

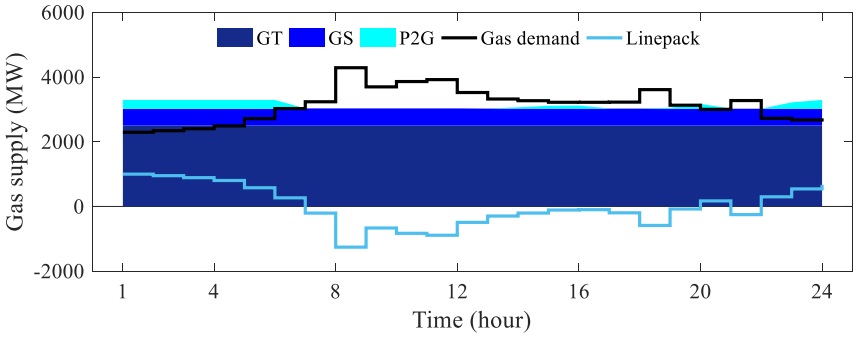

Fig. 45 Optimized gas supply in the natural gas system

Planning of the power-to-gas plants considering the geographic locations

In addition to the previous description on 'which bus should the P2G station be connected to?' the proper geographical locations for P2G stations should also be located near the carbon sources such as biogas stations, etc. **In a drafted paper (attached in the annex entitled 'A Method for Geographic Placement of Power to Gas Plants')**, a geographic information system (GIS) based method to investigate potential locations for power-to-gas plants is also developed. The method determines the location of the plants by considering carbon source potentials, proximity of the grid and costs of grid transmission and investment costs of the technology itself. By combining these types of data, it is possible to identify the investment and operation costs of the power-to-gas plants more accurately. The method focuses on biogas upgrade and CO_2, which are the carbon sources for methanation. A specific case of investigating the power-to-gas potential in Denmark is illustrated in Fig. 46.

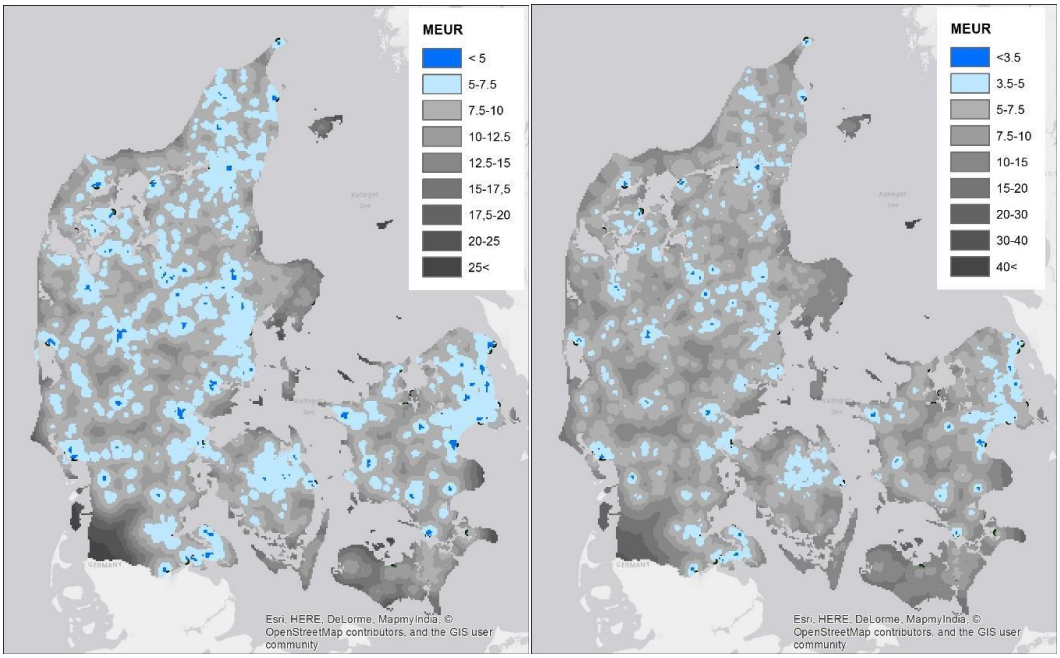

Fig. 46 Illustrative example of GIS planning of P2G plants in 2 different scenarios. (Details can be found in attached manuscript in the annex entitled 'A Method for Geographic Placement of Power to Gas Plants')

The potential is assessed by examining the investment costs of plants with an annual gas production of 60 GWh. The findings of the analysis indicate that the biogas upgrade paths, at the present cost level, is the cheapest path of the two, but due to the relatively small number of biogas plants in Denmark, it is limited to around 55 plants with the chosen plant size. CO_2 methanation is on the other hand more costly, but has a larger potential of around 800 plants. As the analysis is based on the current sources for biogas and CO_2, it is important to mention

that the potential for CO_2 methanation plants can be expected to diminish in the future as more renewable energy is introduced, while biogas production could see an increase.

1.5.2 Project objectives and realising status

Table 7 outlines the project objectives and the relevant achievements. Every achievement results in at least 1 publications. The full publication list is in Section 1.5.5.1.

Table 7 The project objectives and their associated achievements/publications

Project Objectives		**Achievements**	**Resulting Publications**
WP1	**System design and expansion planning**		
1.1	Stochastic models for energy production and consumption and techno-economic evaluation	Stochastic models of energy profiles for techno-economic evaluation	[10]
1.2	Network models and topological analysis for future energy distribution systems with multi-carriers	Network models for future expended energy system	[2]
1.3	Network risk assessment and mitigation methods	Risk assessment and mitigation methods	[2], [4], [13]
1.4	Multi-objective optimization for expansion of the integrated energy systems	Multi-objective optimization for network design and expansion	[5], [11]
WP2	**Efficient and reliable operation strategy**		
2.1	Models and algorithm for optimal energy flows	Optimal energy flow model for integrated energy systems	[3], [4], [9]
2.2	Multi-time period optimal operation of the integrated energy system	Multi-time period optimization formulated	[1], [9]
2.3	Coordinated control strategy	Optimal coordination of various devices optimized	[6], [7], [14]
2.4	Online software tool development	Real-time online optimization algorithms and program developed	[8], [15]

1.5.3 Management of environmental challenges

This project proposed methodologies of system planning and operation can be used to harmonize the integration of gas, heating and power systems and to improve the overall system efficiency and sustainability. The project can contribute to the full exploitation of renewable energy, the reduction of dependency on fossil fuel; the cost effective development of sustainable and secured energy system, therefore, will benefit the actions of managing environmental challenge and developing environmental friendly societies.

With the application of the project proposed models, methods, optimization strategies for planning and operation of the integrated energy systems, it can be expected that the renewable energy can be more effectively used, the energy system investment cost can be

reduced, the overall operational costs across multiple energy systems can be reduced, the efficiency of the overall energy system will be improved, which will contribute to the realisation of Denmark's renewable goal, 100% of renewable energy by 2050, and EU's energy target and climate objective.

The topological analysis of power system and the planning of P2G stations are based on real-Danish energy systems, which can further be easily modified to provide direct guidance for the evolution of Danish energy systems.

1.5.4 Did the project so far result in increased turnover, exports, employment? Do the project partners expect that the project result in increased turnover, exports, employment?

This project aims to enhance the synergies of multiple energy carriers to improve the efficiency and sustainability of the energy systems. Advanced algorithms and control strategies are developed and applied to real-world case studies. The results obtained in this project can help to promote renewable energy development and new energy conversion equipment deployment, which would result in the increase of turnover and employment in renewable-energy-related industrial sectors, energy conversion equipment manufacturers and plants/system developers. The developed methods could enhance the project partners' experience and knowledge, so that the capabilities of playing a stronger role in the international business market.

1.5.5 How has project results been disseminated?

The results obtained from this project have been disseminated in a number of ways, including top journal paper publications, conference presentation and publications, conference key notes etc. some details are as follows.

1.5.5.1 Publications

Journal papers

[1] "Dynamic Optimal Energy Flow in the Integrated Natural Gas and Electrical Power Systems," IEEE Transactions on Sustainable Energy, vol. PP, no. 99, 2017.

[2] "Power system structural vulnerability assessment based on an improved maximum flow approach," IEEE Transactions on Smart Grid, in press.

[3] "Steady-state analysis of the integrated natural gas and electric power system with bi-directional energy conversion" Applied Energy, vol. 184, pp. 1483–1492, 2016.

[4] "Optimal operation of the integrated electrical and heating systems to accommodate the intermittent renewable sources," Applied Energy, vol. 167, pp. 244-254, Apr. 2016.

[5] "A bi-level programming for multistage co-expansion planning of the integrated gas and electricity system," Applied Energy, in press.

[6] "Coordinated Operation of the Electricity and Natural Gas Systems with Bi-directional Energy Conversion," Energy Procedia, vol. 105, pp. 492–497, May 2017.

[7] "The coordinated operation of electricity, gas and district heating systems," Energy Procedia, in press.

Conference papers

[8] "Hybrid Approximate Dynamic Programming Approach for Dynamic Optimal Energy Flow in the Integrated Gas and Power Systems," the 1st IEEE Conference on Energy Internet and Energy system Integration (EI² 2017), Beijing, China, Nov. 2017. (elected as the best paper in the conference)

[9] "Integrated energy flow analysis in a harmonized natural gas and electricity network with bi-directional energy conversion," 10th Conference on Sustainable Development of Energy, Water and Environment Systems, Dubrovnik, Croatia, Sep. 27-Oct. 2, 2015. (Best paper award in the Conference)

[10] "A hidden Markov model representing the spatial and temporal correlation of multiple wind farms," IEEE Power Energy Society General Meeting (PESGM), Denver, Jul. 2015.

[11] "A multistage coordinative optimization for siting and sizing P2G plants in an integrated electricity and natural gas system," 2016 IEEE International Energy Conference (ENERGYCON), Leuven, Belgium, Apr. 2016.

[12] "MILP formulation for the optimal operation of the integrated gas and power system," IEEE Power Energy Society General Meeting (PESGM), 2017.

[13] "A Two-stage Stochastic Programming Approach for Operating Multi-energy Systems," in the first IEEE Conference on Energy Internet and Energy System Integration, 2017. in press.

[14] "Coordination of Battery Energy Storage and Power-to-Gas in Distribution Systems", Protection and Control of Modern Power Systems, vol. 2, no. 1, pp. 38, Nov 2017.

[15] "Dynamic Performance for Joint Operation of Electricity, Gas and District Heating Systems," submitted at the 1st LA Conference on Sustainable Development of Energy, Water and Environment Systems, SDEWES2018.

1.5.5.2 Keynote speeches

2017 International Electrical and Energy Conference (CIEEC2017), Beijing, China
2017 The 12th Annual Electric Power Industry Conference, Pittsburgh, US

Panel presentation
2017 1st IEEE Conference on Energy Internet and Energy System Integration, Beijing, China

1.5.5.3 Conference awards

Two best papers were awarded on 10th Conference on Sustainable Development of Energy, Water and Environment Systems and the 1st IEEE Conference on Energy Internet and Energy system Integration, respectively.

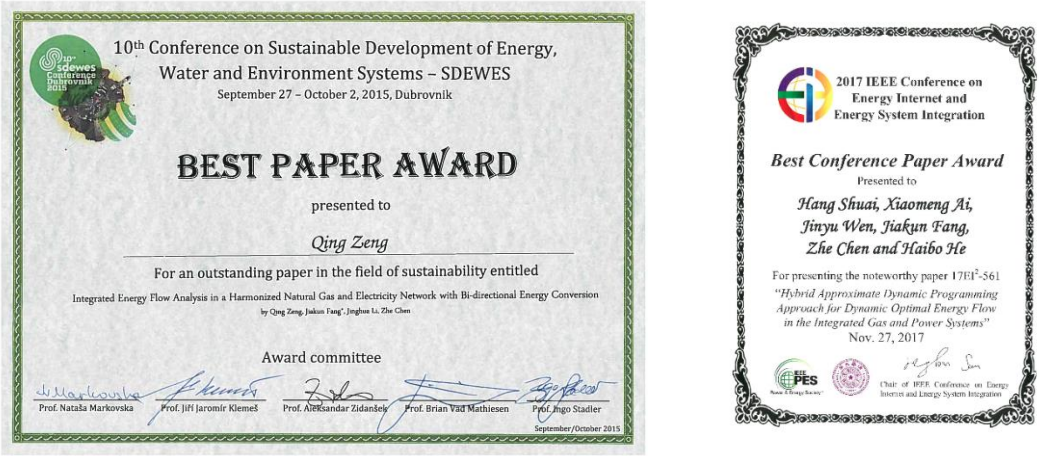

Fig. 47 Best paper awards for this project.

1.5.5.4 Project meetings

In order to ensure the smooth progress of the project, disseminate the research results and get feedback from academic and industrial partners, regular project meetings with all the project partners have been held at Department of Energy Technology, Aalborg University. Other meetings have also been held with industrial partners including Ramboll and Energinet.dk, respectively.

The project has been conducted successfully, the dissemination has been done to create significant positive impacts internationally.

1.6 Utilization of project results

The project results are attracting the attentions from industrial and academic field. The project industrial partner, Ramboll, and advisory committee member, Energinet.dk showed great interests, some concepts and methods developed in the project will provide good knowledge to enhance their work in energy system planning and operation. More importantly, the obtained knowledge will influence the energy sector, with the potential to increase renewable utilisation, to build high efficient and reliable energy system, which and promote the integrated energy system, which is a new stage of the energy system.

The keynotes, panel and paper presentations at conferences have also attracted attentions, the team leader has been invited to give seminars and lectures on this topic by universities and research institutions. The project has already attracted some academic visitors, and more researchers have shown interests in joining the team to have a research stay.

More industry companies are being contacted to promote the technology. The computation tool to be installed on line will further promote the technology, and increase the Danish research influence worldwide.

The project results have been further utilized from following aspects.

Ph.D. course

Based on the findings in this project, the Ph.D. course entitled 'Renewable energy based integrated energy systems' was successfully held in February, 2017. Dr. Jiakun Fang gave a lecture on 'Advanced technologies and emerging facilities for energy system integration and optimization techniques applied in integrated energy systems'.

Visiting scholars

International collaborations are undertaken. AAU-ET hosted a visting scholar Prof. Jinghua Li from Guangxi University during the period December 1st, 2014 to December 1st, 2015.

Project leader, Prof. Zhe Chen has jointly supervised 2 visiting Ph.D. students:

- Hongmin MENG, North China Electric Power University, China, during the period April 4th, 2016 to April 4th, 2017.

- Rui LI, Beijing Jiaotong University, China, during the period October 1st, 2016 – September 30th, 2017.

Graduated Ph.D. and master students

One Ph.D. student Mr. *Qing Zeng* has completed his thesis and scheduled his defence in early 2018.

One Master student, Mr. *Teodor Ognyanov Trifonov* has completed his master thesis entitled 'Coordination of battery energy storage and power-to-gas in distribution systems' and currently working in Industrial company.

Further grant applications

Based on the project work, a number of project applications have been prepared and submitted, including EU H2020 and EUDP/ForskEL projects. An EUDP/ForskEL project (Sustainable Energy Market Integration, project number: 12554) has already been granted.

Special issue or thematic series organized

Project leader, Prof. *Zhe Chen* served as Guest Editor-in-Chief of the special issue on "Enabling very high penetration renewable energy integration into future power systems", IEEE Transactions on Power Systems.

Project participate, Dr. *Jiakun Fang* served as the associated editor of thematic series on "energy storage across multiple energy systems", Protection and Control of Modern Power Systems.

More special issues are in planning.

1.7 Project conclusion and perspective

In this project, the harmonization of gas, heating and power system is comprehensively studied, the technical results are highlighted with 6 main technical achievements. All the working tasks in the proposal are successfully addressed. 15 scientific articles, including 7 journal papers and 8 conference papers, have been published or accepted for publication. 4 interim reports have been completed. 2 special issues are organized in international journals. 1 Ph.D. student and 1 Master student have been educated. 1 visiting professor and 2 joint supervised PhD researchers are hosted in AAU-ET.

The results of the project have demonstrated both academic gains and industrial practical values, the project has set up a good foundation for further investigations on the modelling, optimisation of energy systems, the developed tool can also be further tailored for real energy system planning and operation. Therefore, future developments will be expected in the aforementioned both directions.

Annex

Project website:
http://www.et.aau.dk/research-programmes/wind-power-systems/activities/highe/

List of papers published in international journals and conferences

The publications listed in Section 1.5.5 are all attached.

Interim report and papers ready to submit.

Draft manuscripts:
[1] A Method for Geographic Placement of Power to Gas Plants
[2] District heating and cooling is a cost-effective way to integrate the fluctuating wind energy – it's like a virtual battery

Interim Reports:
[1] Simulating the Danish DH&C Sector
[2] District Heating and Cooling with Thermal Storages - The Virtual Battery
[3] Fjernvarmen er det smarte ellager fjernvarmen nr 6 2017
[4] Integration of wind and solar in the smart energy system